PERFORMANCE ANALYSIS OF AN LDPC CODED FREE-SPACE OPTICAL COMMUNICATION SYSTEM THROUGH ATMOSPHERIC TURBULENCE CHANNEL

A thesis submitted in partial fulfilled of the requirements for the degree of

Master of Science
in
Electrical and Electronic Engineering

By
Bobby Barua

Under the supervision of
Professor Satya Prasad Majumder

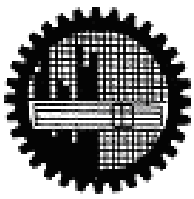

Department of Electrical and Electronic Engineering

Bangladesh University of Engineering and Technology

October 2010

PERFORMANCE ANALYSIS OF AN LDPC CODED FREE-SPACE OPTICAL COMMUNICATION SYSTEM THROUGH ATMOSPHERIC TURBULENCE CHANNEL

A thesis submitted in partial fulfilled of the requirements for the degree of

Master of Science
in
Electrical and Electronic Engineering

By
Bobby Barua

Under the supervision of
Professor Satya Prasad Majumder

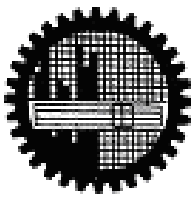

Department of Electrical and Electronic Engineering

Bangladesh University of Engineering and Technology

October 2010

The thesis entitled **"Performance Analysis of an LDPC coded Free-space Optical Communication System Through Atmospheric Turbulence Channel"** submitted by Bobby Barua, Roll no: 040506230P, Session: April 2005 has been accepted as satisfactory in partial fulfillment of the requirements for the degree of **Master of Science in Electrical and Electronic Engineering** on October 9,2010.

BOARD OF EXAMINERS

1. _____
   (Dr. Satya Prasad Majumder) **Chairman**
   Professor
   Department of Electrical and Electronic Engineering
   Bangladesh University of Engineering and Technology
   Dhaka-1000

2. _____
   Dr. Md. Saifur Rahman
   Professor and Head **(Ex-Officio)**
   Department of Electrical and Electronic Engineering
   Bangladesh University of Engineering and Technology
   Dhaka-1000

3. _____
   Dr. Mohammed Imamul Hassan Bhuiyan
   Associate Professor **Member**
   Department of Electrical and Electronic Engineering
   Bangladesh University of Engineering and Technology
   Dhaka-1000

4. _____
   Dr. Md.Hossam-e-Haider
   Wing Commander **Member**
   Instructor Class-A **(External)**
   Department of Elcetrical Electronic and Communication
   Military Institute of Science and Technology
   Mirpur Cantonment, Dhaka-1216

Declaration

I hereby declare that this thesis has been done by me and it or any part of it has not been submitted elsewhere for any other degree or diploma.

Signature of the candidate

(Bobby Barua)
Roll No.:040506230 P

Dedication

To my beloved wife.

Acknowledgement

I am deeply grateful to my supervisor Prof. Satya Prasad Majumder for his consistent guidance, relentless encouragement, helpful suggestions, constructive criticism and endless patience throughout the progress of this research. The successful completion of this thesis would not been possible without persistent motivation and continuous guidance of my honorable supervisor. I wish to express my profound in debt ness and thanks to him for his advice throughout the entire course of this work.

I also grateful to Dr. Md. Saifur Rahman, Professor and Head, Department of Electrical and Electronic Engineering, Bangladesh University of Engineering and Technology (BUET), Dhaka, for providing valuable suggestions on writing a satisfactory thesis.

I also express my profound indebtedness to all my teachers for their continuous encouragement and providing me their helping hand whenever required.

I am also indebted to my family members for their encouragement and patience.

Contents

Chapter 3: Modulation and Coding for Optical Atmospheric Turbulent Channels

Chapter 4: Results and Discussion

Chapter 5: Conclusion and Future work

List of Abbreviations

ANSI	**American National Standards Institute**
BPSK	**Binary Phase shift keying**
BFSK	**Binary frequency shift keying**
BER	**Bit error rate**
EGC	**Equal gain combiner**
FSO	**Free-space optical**
IM/DD	**Intensity modulation direct detection**
LDPC	**Low Density Parity Check**
LED	**Light emitting diode**
MIMO	**Multiple input Multiple output**
MISO	**Multiple input single output**
MLMD	**Multi laser multi detector**
p.d.f	**Probability of density function**
PPM	**Pulse position Modulation**
SISO	**Single input single output**
SIMO	**Single input multiple output**
SEP	**Symbol error probability**
SNR	**Signal to noise ratio**

List of Tables

List of Figures

Abstract

Free-space optical (FSO) communication technology is a promising candidate for next generation broadband networking, due to its large bandwidth potential, unlicensed spectrum, excellent security, and quick and inexpensive setup. FSO has received significant attention recently, as a possible alternative to solve the bottleneck of connectivity problem, and as a supplement to more conventional RF/microwave links. However, optical wave propagation through the air experiences fluctuation in amplitude and phase due to atmospheric turbulence. The intensity fluctuation, also known as scintillation is one of the most important factors that degrade the performance of an FSO communication link even under the clear sky condition. To enable the transmission under the strong atmospheric turbulence, the use of the multi-laser multi-detector (MLMD) concept has been implemented. The use of multiple laser transmitters combined with multiple photo detectors has the potential for combating fading effects on turbulent optical channels. In this thesis, an analytical approach is presented to evaluate the bit error rate performance of a free space optical link using Low Density Parity Check (LDPC) coded Q-ary optical PPM over an atmospheric turbulence channel. Performances are evaluated for multiple-laser and multiple photo-detector combination with and without LDPC code to combat the effect of atmospheric turbulence. The performance results are evaluated in terms of bit error rate (BER) and coding gain for several system parameters. It is found that LDPC coded system provides significant coding gain of 10 to 20dB over an uncoded system at BER 10^{-12} for multiple source and photo-detector combinations.

Chapter 1

Introduction

Chapter 1

Introduction

1.1 Introduction to Communication System

Communications is defined as technology employed in transmitting messages. It is the process of transferring information or message like voice, video, text, data, picture, etc. from one distance to another. The function of communication system is to convey the signal from the information source over the transmission medium to the destination.

1.2 Brief History of Optical Communication

Optical communication systems date back to the 1790s, to the optical semaphore telegraph invented by French inventor Claude Chappe. In 1880, Alexander Graham Bell patented an optical telephone system, which he called the Photophone. However, his earlier invention, the telephone, was more practical and took tangible shape. The Photophone remained an experimental invention and never materialized. During the 1920s, John Logie Baird in England and Clarence W. Hansell in the United States patented the idea of using arrays of hollow pipes or transparent rods to transmit images for television or facsimile systems.

In 1954, Dutch scientist Abraham Van Heel and British scientist Harold H. Hopkins separately wrote papers on imaging bundles. Hopkins reported on imaging bundles of unclad fibers, whereas Van Heel reported on simple bundles of clad fibers. Van Heel covered a bare fiber with a transparent cladding of a lower refractive index. This protected the fiber reflection surface from outside distortion and greatly reduced interference between fibers.

Abraham Van Heel is also notable for another contribution. Stimulated by a conversation with the American optical physicist Brian O'Brien, Van Heel made the crucial innovation of cladding fiber-optic cables. All earlier fibers developed were bare and lacked any form of cladding, with total internal reflection occurring at a glass-air interface. Abraham Van Heel covered a bare fiber or glass or plastic with a transparent cladding of lower refractive index. This protected the total reflection surface from contamination and greatly reduced cross talk between fibers. By 1960, glass-clad fibers had attenuation of about 1 decibel (dB) per meter, fine for medical imaging, but much too high for communications. In 1961, Elias Snitzer of American Optical published a theoretical description of a fiber with a core so small it could carry light with only one waveguide mode. Snitzer's proposal was acceptable for a medical instrument looking inside the human, but the fiber had a light loss of 1 dB per meter. Communication devices needed to operate over much longer distances and required a light loss of no more than 10 or 20 dB per kilometer.

By 1964, a critical and theoretical specification was identified by Dr. Charles K. Kao for long-range communication devices, the 10 or 20 dB of light loss per kilometer standard. Dr. Kao also illustrated the need for a purer form of glass to help reduce light loss.

In the summer of 1970, one team of researchers began experimenting with fused silica, a material capable of extreme purity with a high melting point and a low refractive index. Corning Glass researchers Robert Maurer, Donald Keck, and Peter Schultz invented fiber-optic wire or "optical waveguide fibers" (patent no. 3,711,262), which was capable of carrying 65,000 times more information than copper wire, through which information carried by a pattern of light waves could be decoded at a destination even a thousand miles away. The team had solved the decibel-loss problem presented by Dr. Kao. The team had developed an SMF with loss of 17 dB/km at 633 nm by doping titanium into the fiber core. By June of 1972, Robert Maurer, Donald Keck, and Peter Schultz invented multimode germanium-doped fiber with a loss of 4 dB per kilometer and much greater strength than titanium-doped fiber. By 1973, John MacChesney developed a modified chemical vapor-deposition process

for fiber manufacture at Bell Labs. This process spearheaded the commercial manufacture of fiber-optic cable.

In April 1977, General Telephone and Electronics tested and deployed the world's first live telephone traffic through a fiber-optic system running at 6 Mbps, in Long Beach, California. They were soon followed by Bell in May 1977, with an optical telephone communication system installed in the downtown Chicago area, covering a distance of 1.5 miles (2.4 kilometers). Each optical-fiber pair carried the equivalent of 672 voice channels and was equivalent to a DS3 circuit. Today more than 80 percent of the world's long-distance voice and data traffic is carried over optical-fiber cables.

1.3 Types of Optical Communication

There are two types of optical communication system:

(i) Free Space Optical Communication

(ii) Optica fiber communication

(i) <u>Free Space Optical Communication (FSO)</u>

Free Space Optics (FSO) is a telecommunication technology that uses light propagating in free space to transmit data between two points. The technology is useful where the physical connection of the transmit and receive locations is difficult, for example in cities where the laying of fibre optic cables is expensive. Free Space Optics are additionally used for communications between spacecraft. The optical links can be implemented using infrared laser light, although low-data-rate communication over short distances is possible using LEDs. Maximum range for terrestrial links is in the order of 2-3 km, but the stability and quality of the link is highly dependent on atmospheric factors such as rain, fog, dust and heat. Amateur radio operators have achieved significantly farther distances (173 miles in at least one occasion) using incoherent sources of light from high-intensity LEDs. However, the low-

grade equipment used limited bandwidths to about 4kHz. In outer space, the communication range of free-space optical communication is currently in the order of several thousand kilometers, but has the potential to bridge interplanetary distances of millions of kilometers, using optical telescopes as beam expanders. IrDA is also a very simple form of free-space optical communications.

(ii) Fiber Optic Communication

Fiber-optic communication is a method of transmitting information from one place to another by sending light through an optical fiber. The light forms an electromagnetic carrier wave that is modulated to carry information. First developed in the 1970s, fiber-optic communication systems have revolutionized the telecommunications industry and played a major role in the advent of the Information Age. Because of its advantages over electrical transmission, the use of optical fiber has largely replaced copper wire communications in core networks in the developed world.

The process of communicating using fiber-optics involves the following basic steps: Creating the optical signal using a transmitter, relaying the signal along the fiber, ensuring that the signal does not become too distorted or weak, and receiving the optical signal and converting it into an electrical signal.

1.4 Free Space Optical Communication Systems

The major subsystems in an FSO communication system are illustrated in Fig. 1.1. A source producing data input is to be transmitted to a remote destination. This source has its output modulated onto an optical carrier; typically laser, which is then transmitted as an optic al field through the atmospheric channel. The important aspects of the optical transmitter system are size, power, and beam quality, which determine laser intensity and minimum divergence obtainable from the system. At the receiver, the field is optically collected and detected, generally in the presence of noise interference, signal distortion, and background

radiation. On the receiver side, important features are the aperture size and the f/-number, which determine the amount of the collected light and the detector field-of-view (FOV).

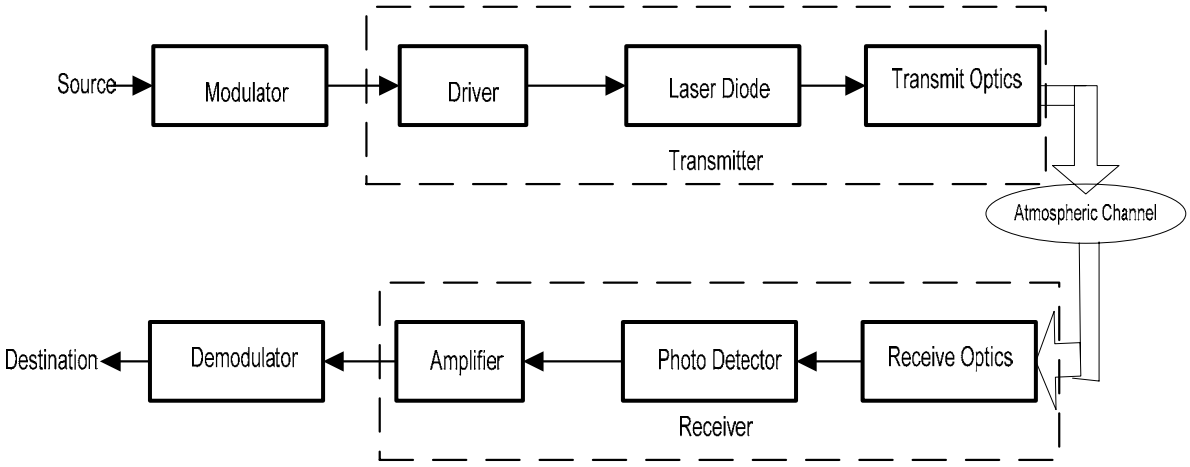

Fig.1.1: Block diagram of FSO communication system.

The modulation of the source data onto the electromagnetic wave carrier generally takes place in three different ways: amplitude modulation (AM), frequency modulation (FM), or phase modulation (PM), each of which can be theoretically implemented at any frequency. For an optical wave, another modulation scheme is also often used, namely intensity modulation (IM). Intensity is defined as flow energy per unit area per unit time expressed in W/m^2, and is proportional to the square of the field amplitude. The light fields from laser sources then pass beam forming optics to produce a collimated beam. This practice is equivalent to providing antenna gain in RF systems. There are two basic types of optical receivers: non-coherent receivers and coherent receivers. Non-coherent receivers directly detect the instantaneous power of the collected optical field as it arrives at the receivers, thus are often called direct or power detection receivers. These receivers represent the simplest type of implementation and can be used whenever the transmitted information occurs in the power variation (i.e. IM) of the optical field. Coherent receivers, better known as heterodyne receivers, optically mix a locally generated light wave field with the received field, and the combined wave is photo detected. These receivers are used when information is modulated onto the optical carrier using AM, FM, or PM, and are essential for FM or PM detection. The detection of optical fields is effected by various noise sources present at the receiver. The three dominant sources in FSO communications are: background ambient light, photo

detector induced noise, and electronic thermal noise in circuits. Although background radiation may be reduced by the use of optical filtering, it still provides significant interference in the detection process. The detector quantum noise originates from the randomness of the photon counting process at the photo detector. The thermal noise can be modeled as additive white Gaussian noise (AWGN), whose spectral level is directly proportional to the receiver temperature.

1.5 Atmospheric Optical Channel

To design a high-performance communication link for the atmospheric free-space optical (FSO) channel, it is of great importance to characterize the channel from the perspective of information and coding theory. The atmospheric free-space channel is a natural medium for outdoor optical wireless communication and has generated significant research attention in the past 10 years as a complement to radio-frequency (RF) links. The free space optical (FSO) atmospheric channel has a wide bandwidth and may support many more users than an RF channel. Most optical wireless links are based on intensity modulation with direct detection, the same technique that is used for state of the art fiber-optics communications. The availability of the optical components used in fiber optics makes outdoor optical links a cost-effective solution for high-rate voice and data communications. Communication in a FSO channel is achieved by a point-to-point connection of two optical transceivers in line of sight. An optical wave propagating through the air experiences random variations in phase and amplitude due to the effects of turbulence. This turbulence is caused by fluctuations in the refractive index of the medium as the latter experiences temperature gradients due to solar heating and wind.

1.6 Atmospheric Turbulent Channel Modeling

A commonly used turbulence model assumes that the variations of the medium can be understood as individual cells of air or eddies of different diameters and refractive indices. In the context of geometrical optics, these eddies may be thought of as lenses that randomly

refract the optical wave front, producing a distorted intensity profile at the receiver of a communication system. The intensity fluctuations are called scintillation, one of the most important factors that limit the performance of an atmospheric FSO communication link. The most widely accepted theory of turbulence is due to Kolmogorov. This theory assumes that kinetic energy from large turbulent eddies, characterized by the outer scale L_0, is transferred without loss to eddies of decreasing size down to sizes of a few millimeters characterized by the inner scale l_0. The inner scale represents the cell size at which energy is dissipated by viscosity. The refractive index varies randomly across the different turbulent eddies and causes phase and amplitude variations to the wave front. Turbulence can also cause the random drifts of optical beams–a phenomenon usually referred to as wandering – and can induce beam focusing.

Outer scale is assumed to be infinite in this study. We consider zero and non-zero inner scale conditions. Understanding the turbulence effects under zero inner scale is important as it represents a physical bound for the optical atmospheric channel and as such it has been of interest to researchers.

1.7 Efficient LDPC Codes

An LDPC code is a linear error-correcting code that has a parity check matrix H with a small number of nonzero elements in each row and column. Although LDPC codes can be defined over any finite field, the majority of research is focused on LDPC codes over GF(2), in which "1" is the only nonzero element. The code is the set of vectors x such that Hx' = 0. Due to the strong reduction in capacity, the probability of bit error can be very high, even for large values of SNR. This renders the atmospheric FSO channel useless, as such high SNR is not attainable in practice. Therefore, powerful error-correction codes are necessary.

We illustrate the LDPC error-correction codes for the FSO channel that can efficiently operate across all turbulence regimes. These codes have codeword lengths 2025 bits and 4320 bits and rates 0.91 and 0.75, respectively. They also have high minimum distances and provide good error-correction performance. The codes have a regular structure and are

designed using the concepts of combinatorial design. These codes have low encoding and decoding complexity, which is a desirable feature for implementation in actual FSO communication systems.

1.8 Review of Previous Works

- In reference [1] it is found that the atmospheric free-space channel is a natural medium for outdoor optical wireless communication.

- However, optical wave propagation through the air experiences fluctuation in amplitude and phase due to atmospheric turbulence [2].

- In reference [3] the author proposed lognormal model for weak turbulence considering the effect of fading and background noise .

- To enable the transmission under the strong atmospheric turbulence the use of the multi-laser multi-detector (MLMD) concept has been reported in Ref. [4, 5 and 6].

- In several publications, MIMO concept itself and different coding techniques [7,8] are studied.

- Due to I.B. Djordjevic [8] low density parity check coded modulation is more efficient rather than other coding technique.

- In reference [8] the simulation of LDPC coded MIMO optical link is reported without considering the effect of channel.

Therefore it is recommended to consider the channel effect of a coded MIMO FSO system in the presence of atmospheric turbulence.

1.9 Objectives of the Thesis

The main objective of this research is to performance analysis of free space optical communication through atmospheric turbulence channel. The main purpose of this thesis is :

(i) To develop the performance analysis for an LDPC coded in FSO link with single input single output (SISO) system and to extend the analysis to MIMO FSO system taking into consideration the effect of atmospheric channel.

(ii) To evaluate the performance results of a LDPC coded MIMO FSO system in the presence of atmospheric turbulence.

(iii) To determine the effectiveness of LDPC codes in presence of atmospheric effect.

(iv) To evaluate improvement in system parameters due to LDPC codes and to find optimum system design parameters of an MIMO FSO atmospheric link.

1.10 Organization of this Thesis

This thesis consists of five chapters. Chapter 1 discusses the purpose and present state of the art of FSO communication and importance of optical wireless communication in communication field in recent years, and main objectives of this work.

In chapter 2, a brief overview of different components and different terminologies used in FSO communication is discussed.

In chapter 3, LDPC codes are discussed. Two popular channel model, lognormal and gamma-gamma turbulence model are presented which are extensively used in wireless communication. Lognormal channel model is used in weak turbulence condition and gamma-gamma model is best suited for moderate and strong turbulence condition. This chapter also highlights techniques and technical details of uncoded and LDPC coded Q-ary pulse position modulation channels through atmospheric turbulance .

In chapter 4, numerical results are presented for different conditions which are theoretically analyzed in chapter 3.

Finally, conclusions and some suggestions for future work are provided in chapter 5.

Chapter 2

Overview of Free Space Optical Communication System

Overview of Free Space Optical Communication System

2.1 Introduction

In this chapter, the free-space optical link is briefly described. First, the importance of free space optical communication system is described then a brief description on the major components of a free space optical link is also allowed. Finally we look at the application of multiple-input, multiple-output (MIMO) techniques to the FSO system using Q-ary pulse position modulation (Q-ary PPM).

2.2 Importance of Free-Space Optical Communication

Communication systems transmit information from a transmitter to a receiver through the construction of a time-varying physical quantity or a signal. A familiar example of such a system is a wired electronic communications system in which information is conveyed from the transmitter by sending an electrical current or voltage signal through a conductor to a receiver circuit. Another example is wireless radio frequency (RF) communications in which a transmitter varies the amplitude, phase and frequency of an electromagnetic carrier which is detected by a receive antenna and electronics. In each of these communications systems, the transmitted signal is corrupted by deterministic and random distortions due to the environment. For example, wired electrical communication systems are often corrupted by random thermal as well as shot noise and are often frequency selective. These distortions due to external factors are together referred to as the response of a communications channel between the transmitter and receiver. For the purposes of system design, the communications channel is often represented by a mathematical model which is realistic to the physical channel. The goal of communication system design is to develop signaling techniques which are able to transmit data reliably and at high rates over these distorting channels. As a medium for

wireless communication, lightwave radiation offers several significant advantages over radio. Lightwave emitters and detectors capable of high speed operation are available at low cast. The lightwave spectral region offers a virtually unlimited bandwidth that is unregulated worldwide. Infrared and visible light are close together in wavelength, and they exhibit qualitatively similar behavior. Both are absorbed by dark objects, diffusely reflected by light colored objects, and directionally reflected from shiny surfaces. Both types of light penetrate through glass, but not through walls or other opaque barriers, so that optical wireless transmissions are confined to the room in which they originate. This signal confinement makes it easy to secure transmissions against casual eavesdropping, and it prevents interference between links operating in different rooms. Thus, optical wireless networks can potentially achieve a very high aggregate capacity, and their design may be simplified, since transmissions in different rooms need not be coordinated. When an optical wireless link employs intensity modulation with direct detection (IM/DD), the short carrier wavelength and large-area square-law detector lead to efficient spatial diversity that prevents multi-path fading. By contrast, radio links are typically subject to large fluctuations in received signal magnitude and phase. Freedom from multi-path fading greatly simplifies the design of optical wireless links.

The lightwave is not without drawbacks however. Because lightwave cannot penetrate walls, communication from one room to another requires the installation of optical wireless access points that are interconnected via a wired backbone. In many applications, there exists intense ambient light noise, arising from sunlight, incandescent lighting and fluorescent lighting, which induce noise in an optical wireless receiver. In virtually al short-range, indoor applications, IM/DD is the only practical transmission technique. The signal-to-noise ratio (SNR) of a direct detection receiver is proportional to the square of the received optical power, implying that IM/DD links can tolerate only a comparatively limited path loss. Often optical wireless link must employ relatively high transmit power levels and operate over a relatively limited range. While the transmitter power level can usually be increased without fear of interfering with other users, transmitter power may be limited by concerns of power consumption and eye safety, particularly in portable transmitters.

2.3 Major Components of Free Space Optical System

A free space optical links consists of a transmitter, FSO communication channels and a receiver as shown in Fig. 2.1.

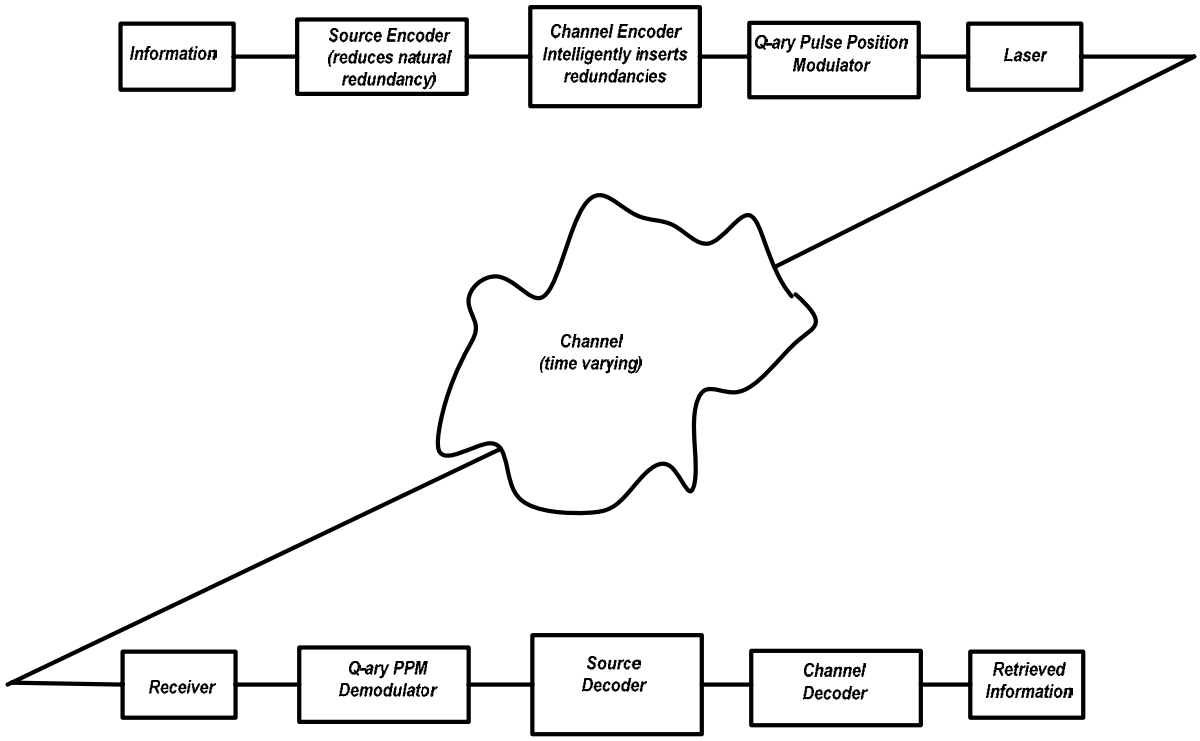

Fig. 2.1: FSO system block diagram.

2.3.1 The Transmitter

In Figure 2.1, the transmitter and modulator are depicted as being separate entities, but there are actually different ways to construct this. It is possible for the transmitter to be constantly on, and then be modulated as it is passed on to the channel, or the laser can be directly modulated in one step.

Here we consider the transmitter to be the light source, which simply has the task of sending light over the channel.

There are three different types of light sources that are commonly used in free-space optics:

- **Light Emitting Diode (LED)**:

LED's can produce light in the 800-900 nm band, they are cheap, and they can produce radiation with low current drive levels. However, they have limited output powers (1-10 mW), there is more frequency spreading than the other light sources, and the light tends to be incoherent and unfocused.

- **Laser:**

Lasers have power outputs of 0.1-1 W, but are much bulkier than LED's. The laser is an optical cavity filled with light amplification material and mirrored facets at each end. When the cavity "lases," an initiated optical field crosses back and forth in a self-sustaining reaction. A small aperture in one of the mirrored facets allows some of the energy to escape as radiated light. In the linear range of operation (see Fig 2.2), lasers are unstable, so they are usually operated as continuous-wave devices at peak power.

- **Laser Diode:**

Like LED's, laser diodes are semiconductor junction devices, but they operate more like lasers with reflecting etched substrates which act like small reflectors (like the reflectors in the laser). Laser diodes are small, rugged, and very power-efficient. They require more drive current than LED's, but also generate more power. A laser diode produces about a hundred milliwatts of useable optical power [10] with a more focused beam than with LED's .

All of the three light sources have the same output power characteristics, shown in Figure 2.2. From this, one can see a distinct linear region of operation, where an increase in input current would result in a proportional increase in output light power.

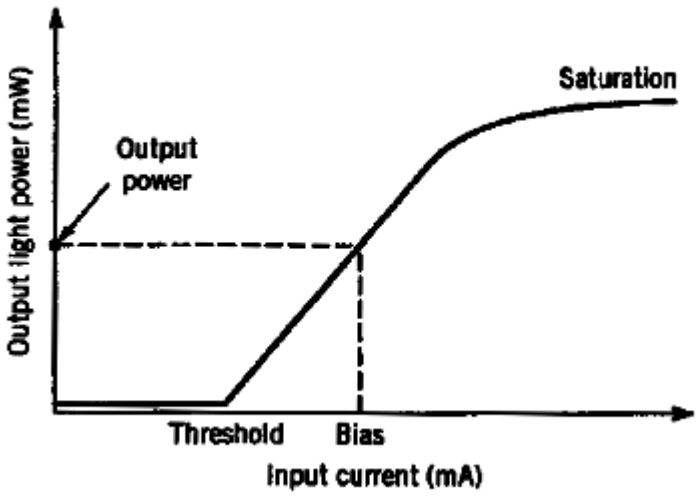

Fig. 2.2: Output light power vs. input drive current for all three most common light sources.

The wavelength chosen for FSO systems usually falls near one of two wavelengths, 850 nm or 1550 nm. The shorter of the two wavelengths is cheaper and is favored for shorter distances. The 1550 nm light source is favored for longer distances since it has an allowed power that is two orders of magnitude higher than at 850 nm [12]. These power limits are determined by the American National Standards Institute (ANSI) Z136.1 Safety Standard [22]. The reason for the higher allowed power is that laser-tissue interaction is very dependent on wavelength. The cornea and lens are transparent to visible wavelengths (such as 850 nm) so the power can reach the retina at the back of the eye. At 1550 nm retinal absorption is much lower, since the power is absorbed mostly by the lens and cornea before it can reach the retina. The power at 1550 nm is not unlimited, however, since it can still cause photo-keratitis and cataracts at higher levels.

The 1550 nm wavelength is also preferred since more photons per watt of power arrive for longer wavelengths, and therefore more photocurrent is produced per watt of incident power for equal efficiency devices.

.

2.3.2 The Receiver

Once the transmitted signal passes through the atmosphere, it must be collected and measured by the receiver. As we mentioned before, both coherent and noncoherent detection schemes are possible, but for complexity and cost reasons noncoherent (or direct detection) is preferred. For this thesis, noncoherent systems are considered only.
In noncoherent optical signal detection, the detectors rely on the photoelectric effect incident photons are absorbed by the detector and free-carriers are generated and can be measured. This is a probabilistic phenomenon, since it is possible for a photon to pass through the photo-detector without generating any free-carriers. However, in a well-designed photo-detector, the probability of an incident photon causing a free-carrier is high [10]. There are two models that we will use in our analysis of the system. In the ideal photon counting model, we assume no thermal noise is present, and the system is capable of counting current 'blips' that occur as each photoelectron is produced. Integrating the photocurrent over a certain period of time (called a 'slot') is equivalent to counting the current 'blips.

In the Gaussian model, it is assume that zero mean, additive white Gaussian noise (AWGN) is added to the generated photocurrent. It is still integrate over a slot, and the integration process should, on average, remove the noise power from the observable.

There are numerous configurations and variations in these four categories, so we will concentrate on the two most popular detectors in optical receivers for communication, p-i-n photodiodes and avalanche photodiodes.

• p-i-n Photodiodes

A p-i-n photodiode is made up of a p-type, and an n-type layer of semiconductor, separated by an intrinsic layer (hence the name p-i-n photodiode). The p-type layer is made to be very thin, so incident photons can pass directly through to the intrinsic region where they can

generate electron-hole pairs. Any pairs that are generated are quickly swept into the p- and n type layers where they contribute to the photocurrent.

The p-i-n photodiode has a quantum efficiency associated with it that depends on the reflectivity of the p-type layer, the absorption length of the intrinsic region, and the length of the depletion region [10]. The quantum efficiency is often denoted by η and is a measure of the average number of electron-hole pairs generated per incident photon. In a practical p-i-n photodiode, ´ ranges from 0.3 to 0.95 [13].
A simplified model of the p-i-n photodiode with its biasing voltage and integrator is shown in Fig. 2.3 below.

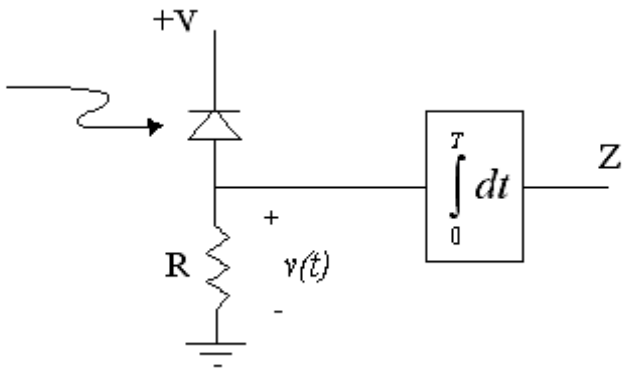

Fig. 2.3: Simplified detector circuit employing a p-i-n photodiode.

- **Avalanche Photodiodes**

An avalanche photodiode (APD) is constructed similarly to a p-i-n photodiode. In some models, there is a second p-type layer between the intrinsic layer and the n-type layer (the layers are p-i-p-n). Incident photons still generate electron-hole pairs, but now there is an "avalanche" effect – each free electron and/or hole has the potential to create more free electrons and/or holes as it traverses the gain region (the extra p-type layer and part of the n-type layer). Each newly created electron or hole can then repeat the process until all carriers have exited the gain region.

This avalanche process creates multiple carriers for every incident photon. This increase in the number of carriers is known as the APD gain. It is the ratio of observable photocurrent at the APD terminals to the internal photocurrent before multiplication [10], and is a random variable with mean G. A simplified model of an APD is shown in Fig. 2.4.

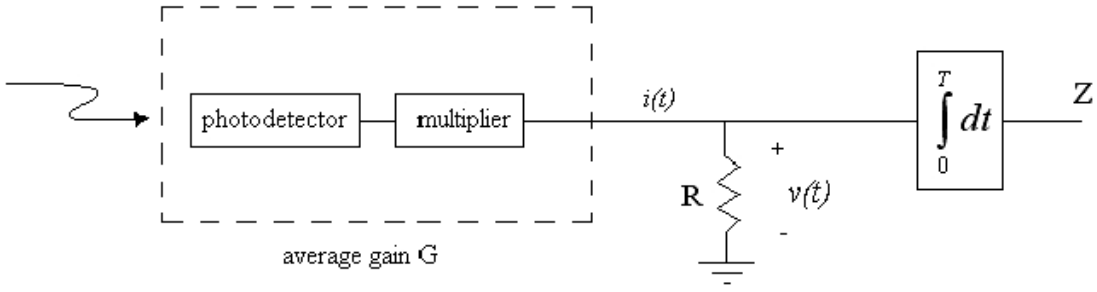

Fig. 2.4: Simplified model of an APD and integrator.

2.3.3 The Channel

In a free-space optical link, the channel is simply the atmosphere plus any other disturbances through which the optical signal will pass. This is a very important component of our system, since the channel is often the limiting factor for how long the link can be.

The atmospheric channel is uncontrolled in that the designers have no way of preventing obstructions and other disturbances from coming between the transmitter and receiver. The engineer will attempt put the system in a location where it is unlikely for obstructions to occur, but it is always possible for a bird, for example, to temporarily pass through the beam. However, in a packet-switched network, short duration interruptions are easily handled by retransmitting the data.

The characteristics of the wireless optical channel can vary significantly depending on the topology of the link considered. This section presents three popular wireless optical channel topologies and discusses the channel characteristics of each.

• Point-to-point Links

Point-to-point wireless optical links operate when there is a direct unobstructed path between a transmitter and a receiver. Fig. 2.5 presents a diagram of a typical point-to-point wireless optical link. A link is established when the transmitter is oriented toward the receiver. In narrow field-of-view applications this oriented configuration allows the receiver to reject ambient light and achieve high data rates and low path loss. The main disadvantage of this link topology is that it requires pointing and is sensitive to blocking and shadowing. The frequency response of these links is limited primarily by front-end photodiode capacitance. Since inexpensive large-area photodiodes are typically used with limited reverse bias the depletion capacitance significantly limits the link bandwidth [14].

A typical example of these links is the standard Infrared Data Association (IrDA) Fast *IR 4Mbps* link. These links offer communication over lm of separation and are used primarily for data interchange between portable devices. The achievable bandwidth in these inexpensive systems is on the order of *10-12MHz* which is approximately three orders of magnitude smaller than in wired fibre-optic systems. New IrDA point-to-point links operating at *16Mbps* have also been standardized and may begin appearing in a wider range of applications.

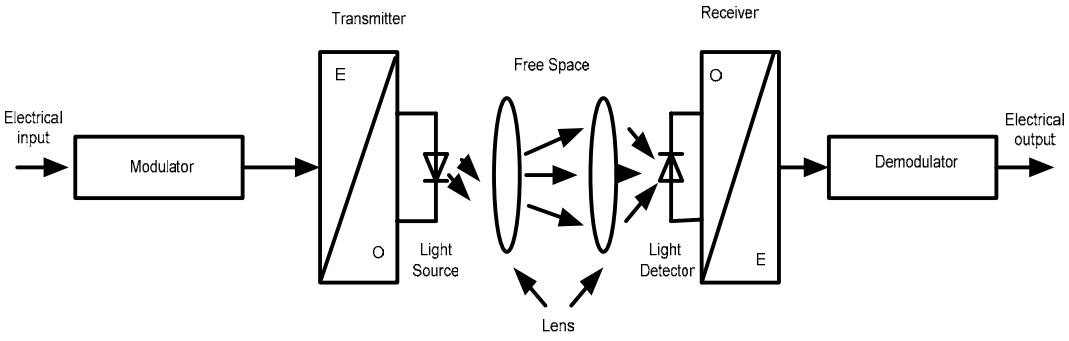

Fig. 2.5: Block diagram of point to point optical link

• Diffuse Links

Diffuse transmitters radiate optical power over a wide solid angle in order to ease the pointing and shadowing problems of point-to-point links. Figure 2.6 presents a block diagram of a diffuse wireless optical system. The transmitter does not need to be aimed at the receiver since the radiant optical power is assumed to reflect from the surfaces of the room. This affords user terminals a wide degree of mobility at the expense of a high path loss. These channels however suffer not only from optoelectronic bandwidth constraints but also from low-pass multipath distortion [15]. Unlike radio frequency wireless channels diffuse channels do not exhibit fading. This is due to the fact that the received photodiode integrates the optical intensity field over an area of millions of square wavelengths and hence no change in the channel response is noted if the photodiode is moved a distance on the order of a wavelength [16]. Thus the large size of the photodiode relative to the wavelength of light provides a degree of spatial diversity which eliminates multipath fading. Multipath distortion gives rise to a channel bandwidth limit of approximately 10-200 MHz depending on room layout shadowing and link configuration [16, 17]. Many channel models based on measurements allow for the accurate simulation of the low-pass frequency response of the channel. The IrDA and the IEEE have similar standards for diffuse infrared links. The IrDA Advanced Infrared (AIr) standard allows communication at rates up to 4 Mbps with repetition coding. Experimental indoor wireless optical links have been demonstrated at 50 Mbps using on-off keying over a horizontal range of approximately 3 m. A commercial indoor diffuse wireless optical link aimed at digital audio and set-top box applications claims data rates of up to 5 Mbps in typical indoor environments. The diffuse link was able to provide data rates of up to 19.2 kbps and was used to communicate electronic mail and other data to a hand-held computing device.

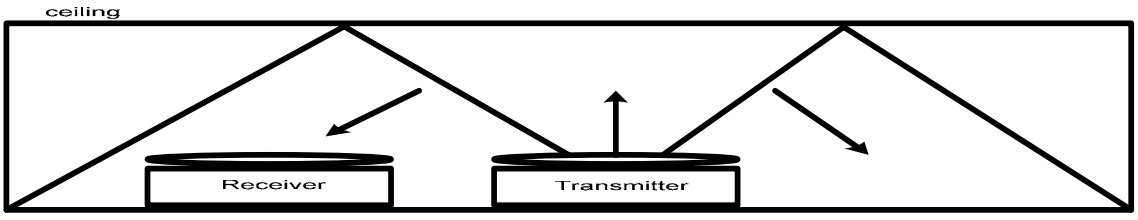

Fig. 2.6: A diffuse optical wireless communication system

•Quasi-Diffuse Links

The transmitter illuminates the ceiling with a series of slowly diverging beam sources which illuminate a grid of spots on the ceiling. In experimental settings these multiple beams are created using individual light sources [18] and techniques using holographic beam splitters appear promising [19]. The transmitted beams suffer a small path loss nearly independent of the length of the link from the transmitter to the ceiling due to the low beam divergence. The data transmitted on all beams is identical. The receiver consists of multiple concentrator/photodiode pairs, each with a non-overlapping narrow FOV of the ceiling. The FOV of each receiver is typically set to see at least one spot on the ceiling. These narrow FOV receivers reject a majority of multipath distortion and provide a link with an improved bandwidth although the link is more sensitive to shadowing relative to diffuse links. Spatially localized interferers such as room illumination can be rejected by using the spatial diversity of the multiple receivers. In a diffuse scheme, all the noise power is collected along with the signal power.

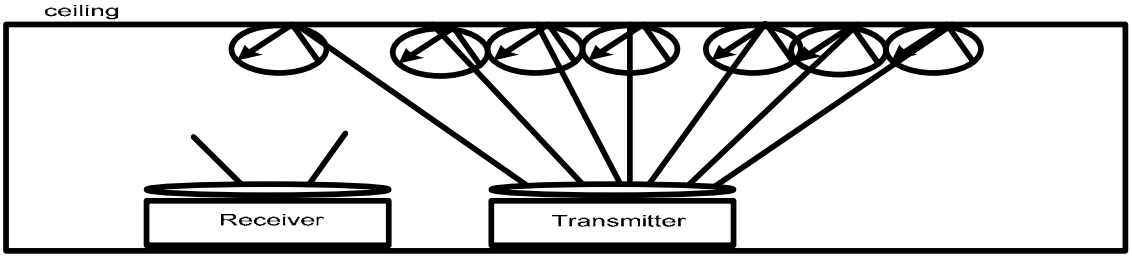

Fig. 2.7: A quasi-diffuse optical wireless communication system

Table 2.1 Comparison of wireless optical topologies

	Point to point	Diffuse	quasi-diffuse
Rate	High	Low-Moderate	Moderate
Pointing Required	Yes	No	Somewhat
Immunity to Blocking	Low	High	Moderate-High
Mobility	Low	High	Moderate-High
Complexity of Optics	Low	Low-Moderate	High
Ambient Light Rejection	High	Low	High
Multipath Distortion	None	High	Low
Path Loss	Low	High	Moderate

Table 2.1 presents a comparison of some of the characteristics of the three channel topologies discussed. The point-to-point topology is a low complexity means to achieve high data rate links at the expense of mobility and pointing requirements. Diffuse links suffer from high path loss but offer a great degree of mobility and robustness to blocking. Quasi-diffuse links permit higher data rates by requiring users to aim their receivers at the ceiling but suffer from a higher implementation cost due to the multi-beam transmitter. Thus each channel topology is suited to a different application depending on required data rates and channel conditions. It may also be advantageous to combine the operation of the various topologies to form a more robust link. Recent work has demonstrated experimental configurations which use a diffuse wireless optical channel to aid in acquiring tracking and to serve as a backup link to improve user mobility [20].

2.4 Atmospheric Effects on the FSO Channel

A more serious threat is the atmosphere itself. Zhu and Kahn classify atmospheric effects on the FSO channel into two categories, atmospheric turbulence and aerosol scattering [9]. These are discussed further below.

2.4.1 Turbulence

Atmospheric turbulence is also known as scintillation. Even on a clear day, there are continual variations in the intensity of the light at the receiver due to inhomogeneities in the temperature and pressure of the atmosphere. The Kolmogorov turbulence model is often used to describe atmospheric turbulence [9, 21] and predicts that changes in the air temperature as small as 1 degree Kelvin can cause refractive index changes as large as several parts per million [21]. These pockets of air with different refractive indices, or eddies, act like time varying prisms [12] whose size ranges from a few millimeters to a few meters [9], and whose time scale is related to wind speed among other things.

These eddies cause the light to diffract along the path to the receiver in a time-varying manner, affecting the intensity of the light. This phenomenon is visible to the naked eye by

watching the stars twinkle at night, or by watching the horizon shimmer on a hot day [12]. The effect of scintillation on a FSO communications link can be a wandering beam when the eddies are bigger than the beam diameter and move the beam completely off target [12], fluctuating power at the receiver [22], and changes in the phase of the received light wave [9].

For weak turbulence, the intensity of the received signal is a random variable best approximated by a log-normal distribution. To describe turbulence-induced fading, we do so using parameters in the spatial and temporal domains. The first useful parameter is the correlation length, which we call d_0. This is simply the distance for which the intensity of a light wave at two points in the atmosphere is essentially uncorrelated. This distance can be approximated by $d_o \approx \sqrt{\lambda L}$, where λ is the wavelength of the transmitted wave, and L is the length of the FSO link [12]. This approximation is valid for most FSO communication systems using visible or infrared lasers for link lengths ranging from a few hundred meters to a few kilometers [9], and is approximately 1-10 cm for most terrestrial links [12]. The importance of correlation distance will become evident as we talk about spatial diversity as a method of mitigating the effect of turbulence on FSO links.

The second useful parameter is the correlation time, which we call τ_0. When observing a single point in the atmosphere at two different times, τ_0 represents the amount of time between observations for which the atmospheric parameters are uncorrelated. The time scale for scintillation is about the time it takes a volume of air the size of the beam to move across the path, and is therefore related to wind speed. Typical values for terrestrial links are 1-10 ms [12]. Correlation time is important to our discussion in order to justify spatial diversity as a method of mitigating block fading. At the transmission rates desirable for a FSO system (2.5 Gbps for example), a deep fade that could last 1-10 ms could potentially affect 2.5 to 25 megabits of data. The normal approach to counteract block fades is to interleave the data before coding, but this is an unattractive solution due to the enormous size of the interleaver that would be necessary to be effective [21].

2.4.2 Aerosol Scattering

The most detrimental atmospheric phenomenon that affects FSO links is fog, which is classified as aerosol scattering. According to Acampora, susceptibility to fog has slowed the commercial development of free-space optics, since it so severely limits the range of a FSO link. The exact amount of signal attenuation caused by fog varies with its density. Acampora states that the link might lose 90% of its power for every 50 meters in moderately dense fog [23]. This translates into a loss of 200 dB/km. Other sources give ranges in attenuation from 16 dB/km in light fog [22] to 300 dB/km in dense fog.

There are various ways to combat link fade due to fog. One such method is to simply increase the power, also known as increasing the link margin. The link margin is simply extra transmit power that is in excess of what is normally needed to communicate. The only problem with increasing the link margin is that power levels are limited for any system, both because of eye safety as well as practical limitations in the system itself. For moderately dense fog, increasing the link power by a large amount, 60 dB (a factor of one million) for example, would still only allow for an extra 300 m in link length.

Fading can also be mitigated by making the link length as small as possible. Longer links can be accommodated by arranging the transmitters and receivers in a mesh-topology. In an urban setting, the mesh could jump from building-to-building or house-to-house, so that the signal propagates only over shorter distances and has multiple paths to reach any point in the network [23].

The wavelength of the link also affects the link's susceptibility to fog. Future FSO systems will most likely take advantage of the long wavelength infrared range (LWIR) spectrum ($8\mu m < \lambda < 14\mu m$), also known as the night-vision spectrum. LWIR systems are called all weather systems because they are 10-20 times less sensitive to fog, rain, smog, and other atmospheric disturbances. These wavelengths are also far less dangerous to eye safety so allowable power levels are higher than those for the 0.7-1.55 μm range. [18]. Point-to-point microwave radio is an alternative to free-space optics that is immune to fog. However, this

technology requires spectrum licensing, which is a major disadvantage when compared to FSO systems [23].

Effectively overcoming challenges imposed by foggy weather for any particular FSO link would most likely involve a combination of the aforementioned solutions. Using spatial diversity to combat atmospheric effects, which is the focus of this thesis, can be incorporated into almost any well-designed system that also uses link margin, a mesh topology, and LWIR lasers. The effect of also using spatial diversity is to introduce yet one more weapon in the arsenal of the communications engineer to combat link fading.

2.4.3 Fading Models

There are three widely used models for fading. These are Rayleigh distribution ,log-normal distribution and Gamma-gamma distribution. In all of the fading cases, we keep the expected path gain $E[A^2]$ equal to one. The log-normal distribution is very often used in the literature to describe atmospheric turbulence as experienced in FSO systems. In the log-normal distribution, the amplitude of the path gain is a random variable $\boldsymbol{A}$ where $\boldsymbol{A = e^x}$ and $\boldsymbol{X}$ is normal with mean μ_x and varianc σ^2_x .[1]. The Rayleigh distribution is used less often in the literature than log-normal fading to analyze FSO systems, but has some nice properties that make it an attractive model to use. First of all, the Rayleigh fading case exhibits deeper fading than log-normal fading because of the higher concentration of low-amplitude path amplitudes. Second, with Rayleigh fading, the diversity order of the MIMO system becomes apparent when analyzing the slopes of the curves for symbol error probability [9], in order to make fair comparisons between them and the non fading case. With increasing path length or in homogeneity strength, the focusing effect is weakened by multiple self-interference and the fluctuations slowly begin to decrease, saturating at a level for which the scintillation index approaches unity from above.

MIMO Optical Communication

The use of multiple lasers at the transmitter and multiple photo detectors at the receiver in free space optical systems, popularly known as MIMO (multiple-input multiple-output) technology, has rapidly gained in popularity over the past decade due to its powerful performance-enhancing capabilities. Communication in wireless channels is impaired predominantly by multi-path fading. Multi-path is the arrival of the transmitted signal at an intended receiver through differing angles and/or differing time delays and/or differing frequency (i.e., Doppler) shifts due to the scattering of electromagnetic waves in the environment. Consequently, the received signal power fluctuates in space (due to angle spread) and/or frequency (due to delay spread) and/or time (due to Doppler spread) through the random superposition of the impinging multi-path components. This random fluctuation in signal level, known as fading, can severely affect the quality and reliability of free space optical communication.

Optical MIMO technology constitutes a breakthrough in free space communication system design. The technology offers a number of benefits that help meet the challenges posed by both the impairments in the wireless channel as well as resource constraints. In addition to the time and frequency dimensions that are exploited in conventional single-transmitter (single-input single-output) wireless systems, the leverages of MIMO are realized by exploiting the spatial dimension.

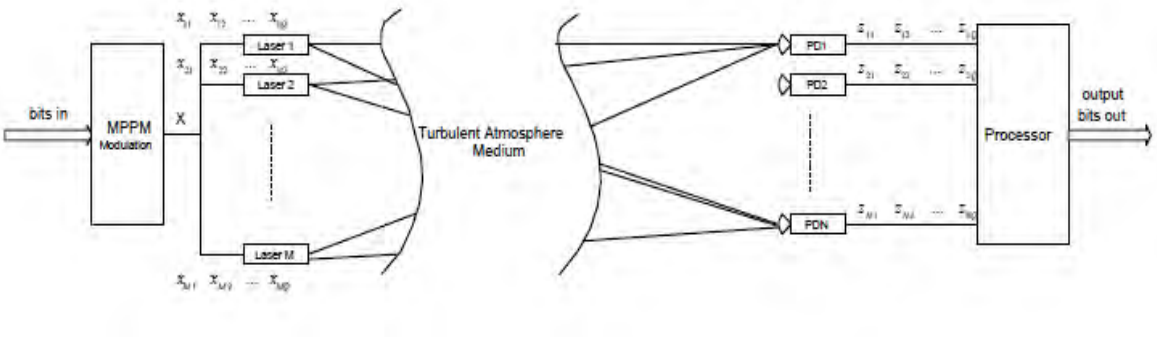

Fig. 2.8 Free space optical MIMO system model

2.5.1 Benefits of MIMO Technology

- MIMO technology has rapidly gained popularity due to its powerful performance-enhancing capabilities.
- The benefits of MIMO technology that help achieve such significant performance gains are *array gain*, *spatial diversity gain* and *spatial multiplexing gain.*
- MIMO systems offer a linear increase in data rate.
- MIMO technology also reduce the bit error rate of the system.
- Interference may be mitigated in MIMO systems by exploiting the spatial dimension. to increase the separation between users.
- Low impact installation.
- Unlicensed use.

2.5.2 Limitations of Optical MIMO Wireless System

- Pointing miss alignment error.
- Strong effect in Fog.
- Strong wind may reduce the performance.
- Performance should decrease for thermal noise.
- Atmospheric turbulences have strong effect on MIMO wireless system.

2.5 Intensity Modulated Direct Detection (IM/DD) Systems

For optical wireless communication systems, most frequently used system is Intensity Modulated Direct Detection *(IM/DD)* system. In optical wireless systems, the intensity of an optical source is modulated to transmit signals. For digital data transmission, there is no practical alternative to digital modulation since it provides source coding (data compression), channel coding (error detection/correction), and easy multiplexing of multiple information streams [21]. The transmission of the digital data can be done on a bit-by-bit basis (binary encoding) or on a bit-word basis (block encoding). Several baseband modulation schemes for

binary and block encoding are discussed; and their performance in terms of power and bandwidth efficiency is compared.

The simplest type of binary modulation scheme is OOK. In an active high OOK encoding, a '1' is coded as a pulse, while a '0' is coded as no pulse or off field. To restrict the complexity of the modulator, the pulse shape is chosen to be rectangular. Modulation in which the temporal positions of the pulses are varied in accordance with some characteristic of the modulating signal. One of the most commonly used optical block encoding schemes is PPM, where an input word is converted into the position of a rectangular pulse within a frame. QPPM is an energy-efficient and readily implemented modulation choice for optical communication. In this method, a signaling interval of length T_s is subdivided into **Q** slots, each of length $T = T_s / Q$ and digital message comprised of $\log_2 Q$bits is sent by pulsing the laser in one of these slots. QPPM is advocated over a simpler binary on–off modulation for another reason; the receiver does not require careful threshold adjustment that tracks the received power level to make optimal decisions.

2.6 Expression of Bit Error Rate (BER):

In any communication system the BER is the most important factor. A standard BER in communication system some times is maintained. For video, speech, data and for every information the separate BER is maintained. BER is related to the input signal power and also SNR. As the input signal power increases the BER decreases.

$$BER = \frac{Number\ of\ bits\ received\ with\ error}{Total\ number\ of\ bits}$$

The required SNR to maintain particular bit error rates may be obtained using procedure adopted for error performance of electrical digital systems where the noise distribution is considered to be white Gaussian. This Gaussian approximation is sufficiently accurate for design purposes and is far easier to evaluate than the more exact probability distribution within the receiver.

Two types of noises, such as, thermal noise and shot noise are considered and also assumed that all these noises have Gaussian distribution. It is assumed that lights from all optical sources have an identical state of polarization, which corresponds to considering the worst case situation for system degradation.

.

2.7 Summary

This chapter addresses the major components of a free space optical link. Analysis are extended to the key concepts and challenges in designing and understanding the performance limits of a free space optical MIMO communication system based on Q-ary Pulse Position Modulation.

Chapter 3

Modulation and Coding for Optical Atmospheric Turbulent Channels

Modulation and Coding for Optical Atmospheric Turbulent Channels

3.1 Introduction

This chapter highlights techniques and technical details of uncode and LDPC coded modulation employing Q-ary pulse position moddulation through atmospheric turbulance channels. We review each of the two channel models used throughout the thesis and discuss their relations among them.

3.2 Free Space Channel Model

Atmospheric turbulence can degrade the performance of free-space optical communication systems, particularly over ranges longer than 1 *km* [1]. Inhomogeneities in the temperature and pressure of the atmosphere lead to variations in the refractive index along the transmission path. These index inhomogeneities cause fluctuations in both the intensity and the phase of the received signal [2]. As a consequence, these fluctuations lead to an increase in the system error probability, limiting the performance of the communication system.

Though we assume an LOS path exists between the transmitter and receiver array, the transmitted field from a single laser will propagate through an atmosphere and may experience several effects [3]. First, electromagnetic scattering from water vapor and other molecules causes a redirection of the optical energy, with corresponding loss of signal power at the receiver. Normally, this is only a significant effect if the water vapor content (and drop size) becomes large, or if substantial haze conditions exist.

A second phenomenon is refraction on a more macroscopic scale. Here, small regions of density in homogeneity in the atmosphere, due to pressure and/or temperature gradients, create a non uniform index of refraction throughout the medium. This is especially prominent on optical links parallel to and near the ground. Even though these regions can be treated as lossless, the aggregate field received at some point in the plane of the PDs becomes a random variable. This field strength is a function of space and also time, due to assumed turbulence of the medium. Several models exist for the aggregate amplitude distribution, though none is universally accepted, since the atmospheric conditions obviously matter. Most prominent among the models are the log-normal , Rayleigh and gamma-gamma model.

3.2.1 Log-normal and Rayleigh Model

For propagation distances less than a few kilometers, variations of the log-amplitude are typically much smaller than variations of the phase. Over longer propagation distances, where turbulence becomes more severe, the variation of the log amplitude can become comparable to that of the phase. Based on the atmosphere turbulence model adopted here and assuming weak turbulence, we can obtain the approximate analytic expression for the covariance of the log-amplitude fluctuation of plane and spherical waves which is also known as Rytov variance, given by[2],

$$\sigma_R^2 = 1.23 C_n^2 k^{7/6} L^{11/6} \tag{3.2.1}$$

where C_n^2 is the wave number spectrum structure parameter and depends on the altitude.

Due to the turbulence of the atmosphere, the field strength received at the detector becomes a random field. We adopt both log-normal and Rayleigh models - which are the most accurate among them. In the log-normal model, the amplitude of the random path gain **A** can be written as $\mathbf{A}=\mathbf{e}^{\mathbf{x}}$, where **X** is normal with mean $\boldsymbol{\mu}_{\mathbf{x}}$ and variance $\boldsymbol{\sigma}^2_{\mathbf{x}}$. By definition, the logarithm of *A* follows a normal distribution. The p.d.f. of *A* is given by [1],

$$f_A(a) = \frac{1}{(2\pi\sigma_x^2)^{\frac{1}{2}} a} \exp\left(-\frac{(\log_e a - \mu_x)^2}{2\sigma_x^2}\right), a > 0 \tag{3.2.2}$$

Thus, the logarithm of the field amplitude-scale factor is normally distributed. (This also means that the optical intensity, proportional to $\mathbf{A^2}$is log-normally distributed.) Since the mean path intensity is unity, i.e. $\mathbf{E[A^2]=1}$, we require $\boldsymbol{\mu_x = -\sigma^2_x}$. The scintillation index (S.I.), a measure of the strength of atmospheric fading, known to information theorists as the "amount of fading", is defined as

$$S.I. = \frac{E\left[A^4\right]}{E^2\left[A^2\right]} - 1 \tag{3.2.3}$$

which, for lognormal distribution, can be shown to equal $S.I. = 4e^{\sigma_x^2} - 1.$ Typical values appearing in the literature are S.I. in the range of 0.4–1.0.

Rayleigh fading emerges from a scattering model that views the composite field as produced by a large number of non dominating scatterers, each contributing random optical phase upon arrival at the detector. Furthermore, with Rayleigh fading, the diversity order which means the number of independently fading propagation paths - of the MIMO system becomes apparent by analyzing the slopes of the symbol error probability curves . The p.d.f of *A* under the Rayleigh distribution is

$$f_A(a) = 2a e^{-a^2}, \; a > 0 \tag{3.2.4}$$

The central limit theorem then gives a complex Gaussian field, whose amplitude is Rayleigh. In this case, the random intensity $\mathbf{G=A^2}$ is a one-sided exponential random variable, or chi-squared with two degrees of freedom.

We again normalize so that $\mathbf{E\ [A^2]\ =1}$, giving **S.I.=1** for the Rayleigh case, though the distribution is quite different from the log-normal case, especially in the small-amplitude tail. Fig. 3.2 shows probability density functions (p.d.fs) for the Rayleigh and log-normal cases with two typical values of S.I.

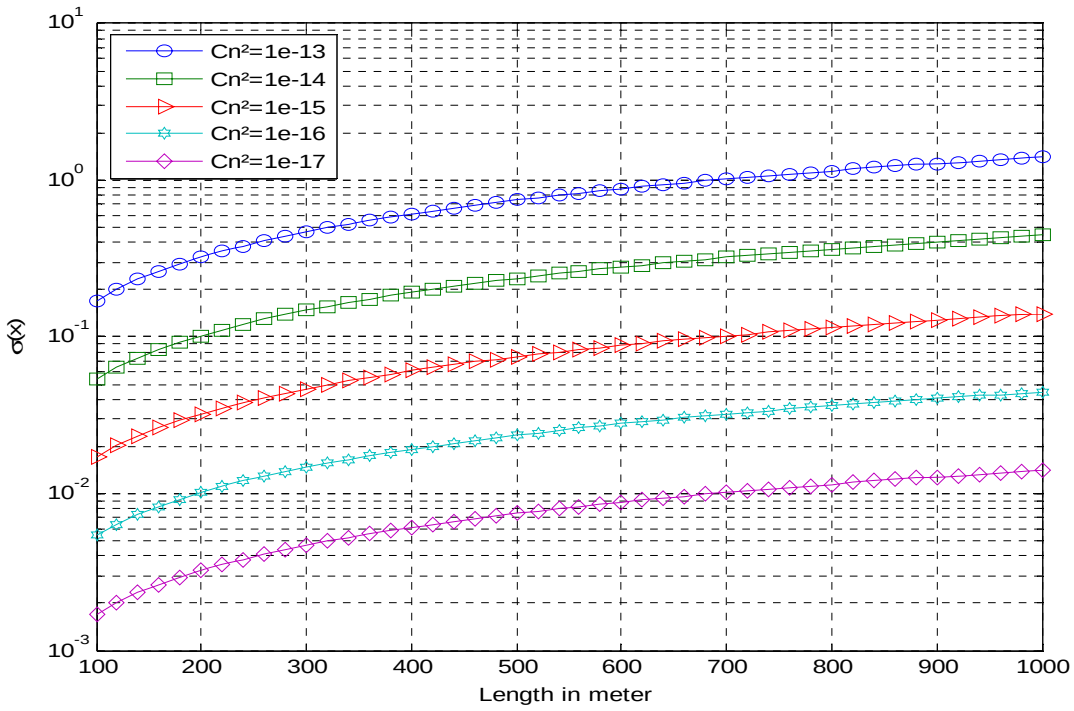

Fig.3.1: Standard deviation of the log-amplitude fluctuation versus propagation distance for a plane wave

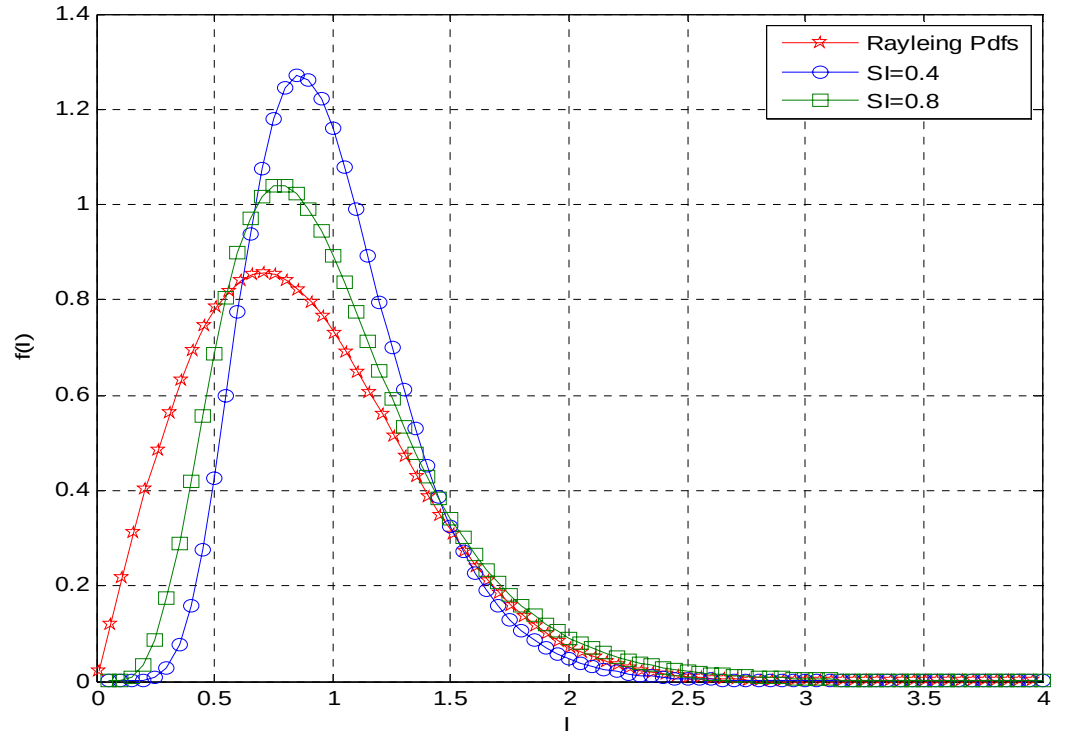

Fig.3.2: Lognormal and Rayleigh p.d.fs

3.2.2 Gamma-gamma Model

Under weak fluctuation conditions, the scintillation index [Eq. (3.2.3)] increases with increasing values of the Rytov variance [Eq. (3.2.1)]. The scintillation index continues to increase beyond the weak fluctuation regime and reaches a maximum value greater than unity (sometimes as large as 5 or 6) in the regime characterized by random focusing. With increasing path length or in homogeneity strength, the focusing effect is weakened by multiple self-interference and the fluctuations slowly begin to decrease, saturating at a level for which the scintillation index approaches unity from above.

The irradiance of the received optical wave is modeled as a product $I = I_x\, l_y$, where I_x arises from large-scale turbulent eddies and I_y from small scale eddies. It is assumed that I_x and I_y are statically independent random processes for which the second moment of irradiance is

$$I^2 = I_x^2\, I_y^2 \tag{3.2.5}$$

The reliability of the communication link can be determined if we use a good probabilistic model for the turbulence. Several probability density functions (p.d.fs) have been proposed for the intensity variations at the receiver of an optical link. Al-Habash et al. [24] proposed a statistical model that factorizes the irradiance as the product of two independent random processes each with a Gamma p.d.f. The p.d.f of the intensity fluctuation is given by [8],

$$f(I) = \frac{2(\alpha\beta)^{(\alpha+\beta)/2}}{\Gamma(\alpha)\Gamma(\beta)} I^{\frac{(\alpha+\beta)}{2}-1} K_{(\alpha-\beta)}(2\sqrt{\alpha\beta I}), I > 0 \tag{3.2.6}$$

where I is the signal intensity, α and β are parameters of the p.d.f, Γ is the gamma function, and $K_{\alpha-\beta}$ is the modified Bessel function of the second kind of order $\alpha-\beta$. Here, α and β are the effective number of small-scale and large scale eddies of the scattering environment. These parameters can be directly related to atmospheric turbulence is as[8],

$$\alpha = \frac{1}{\exp\left[\frac{0.49\sigma_R^2}{(1+1.11\sigma_R^{12/5})^{7/6}}\right]-1}, \beta = \frac{1}{\exp\left[\frac{0.51\sigma_R^2}{(1+0.69\sigma_R^{12/5})^{5/6}}\right]-1} \tag{3.2.7}$$

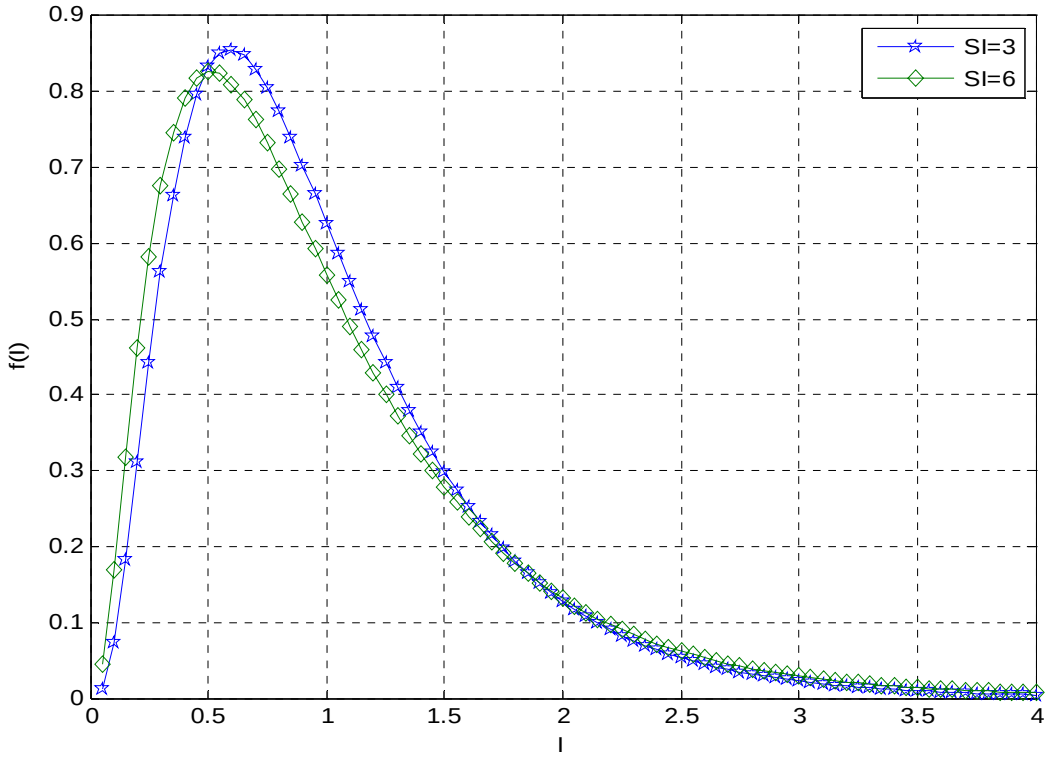

Fig.3.3: Gamma-gamma p.d.fs

3.3 Performance Analysis of an Uncoded FSO Communication System

3.3.1 System Model for SISO FSO System

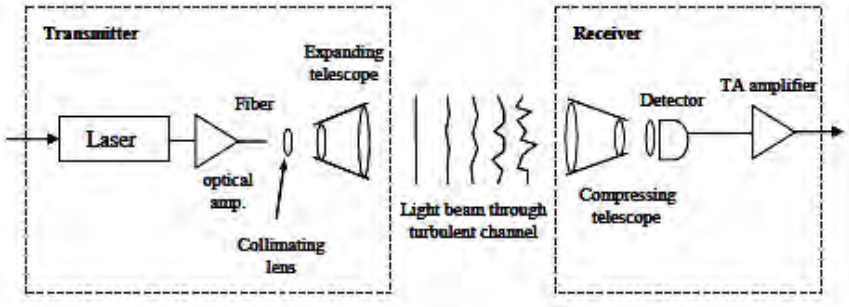

Fig. 3.4 Diagram of the free space optical SISO system model.

A free-space optical communication system is composed of three basic parts: a transmitter, the propagation channel and a receiver. Figure 3.4 shows the block diagram of the free space optical SISO system.

3.3.2 System Model for MIMO FSO System

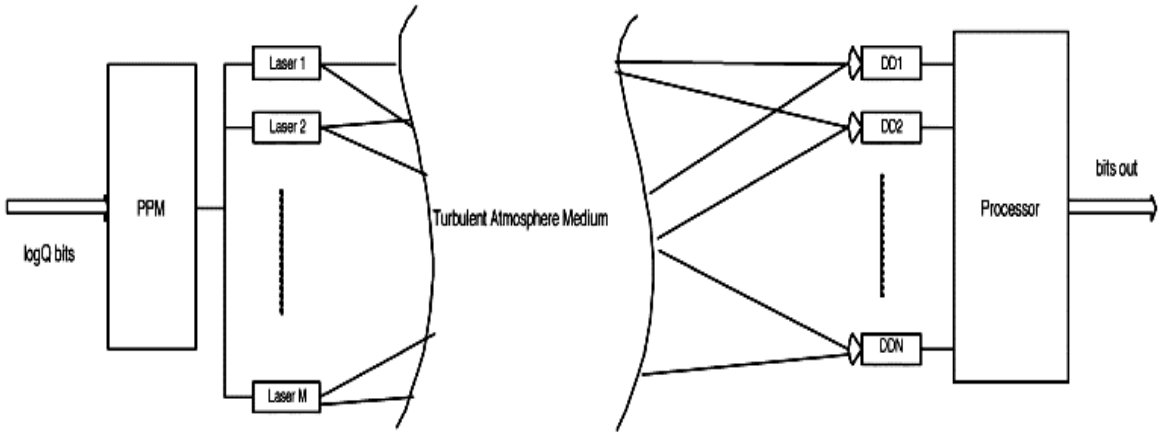

Fig 3.5: Atmospheric optical MIMO system model.

A free-space optical communication system is composed of three basic parts: a transmitter, the propagation channel and a receiver. Fig 3.5 shows the block diagram of the free space optical MIMO system. In the system, ***M*** lasers, intensity-modulated by input symbols, all point toward a distant array of *N* photodetectors. Every laser beamwidth is sufficiently wide to illuminate the entire photodetector array. The ***MN*** laser-photodetector path pairs may experience fading and the amplitude of the path gain from laser ***m*** to detector ***n*** is designated as a_{nm}.

3.3.3 Q-ary Pulse Position Modulation

Pulse-position modulation, or PPM, is a powerful and widely used technique for transmitting information over an optical direct-detection channel [1]. PPM is a modulation technique that uses pulses that are of uniform amplitude and width but displaced in time by an amount depending on the data to be transmitted. It is also sometimes known as pulse-phase modulation. It has the advantage of requiring constant transmitter power since the pulses are of constant amplitude and duration. PPM also has the advantage of good noise immunity since all the receiver needs to do is detect the presence of a pulse at the correct time; the duration and amplitude of the pulse are not important.

The transmit pulse shape for Q--PPM is given by [21] ,

$$p_m(t) = \begin{cases} 1\ , \ for\ t \in [(m-1)T_s / Q, mT_s / Q] \\ 0\ , \ elsewhere \end{cases} \tag{3.3.1}$$

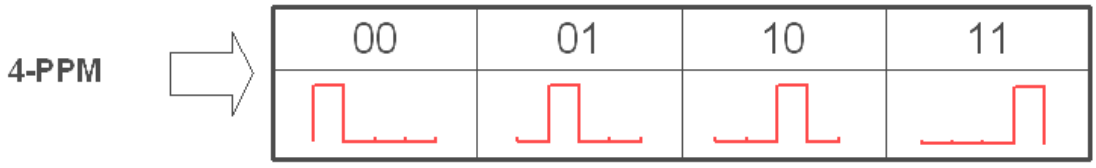

where $m \in \{1,2,....,Q\}$ Since Q possible pulse positions code for $\log_2 Q$ bits of information, the bit rate is $R_b = \log_2 Q / T_s$

Q-ary Pulse Position Modulation, or QPPM, is an energy-efficient and well developed modulation method. At the transmitter, the encoder maps blocks of ***L*** consecutive binary data bits into a single PPM channel symbol by placing a laser pulse into one of several time slots. In this method, every symbol interval of duration $\boldsymbol{T_s}$ is subdivided into ***Q*** slots, each of duration $\boldsymbol{T_Q = T_s/Q}$. If each bit is $\boldsymbol{T_b}$ seconds in duration, then ***L*** bits take $\boldsymbol{T_s = L\ X\ T_b}$ seconds to transmit. We use Q-ary PPM in our system, which means that in every symbol the lasers turn on for ***w*** time slots out of a possible ***Q*** time slots. Of course, $\boldsymbol{w = 1}$ represents conventional QPPM described above. Instead of sending a single pulse as in traditional QPPM, ***w*** pulses are sent in certain symbol slots to transfer a digital message. Every symbol represents $\boldsymbol{L = \log_2(Q/W)}$ bits. This $\boldsymbol{T_s = T_b \log_2(Q/W)}$ where $\boldsymbol{T_b}$ is the bit duration. After establishing the slot and symbol synchronization, the receiver detects the un-coded Q-ary PPM symbols by determining which ***w*** out of the ***Q*** slots contains the laser pulses, and performs the inverse mapping operation to recover the bit stream. If $\boldsymbol{E_b}$ is the energy per bit, then the symbol energy is $\boldsymbol{E_s = E_b \log_2(Q/W)}$. In this thesis, we assume repetition coding across all lasers, that is, each of the M lasers transmits the same ***w***-pulse symbol at the same time. While this constraint restricts the permissible bit rate, relative to an unconstrained set of patterns, the receiver processing is simple, performance analysis is more direct.

3.3.4 Transmitter for Uncoded System

In the transmitter, binary data bits are converted into a stream of pulses corresponding to QPPM symbol described below, and sent to the *M* lasers. The signals are described by the waveforms

$s_0(t)=A=\sqrt{2}P,\ 0\leq t\leq Ts/4$ '00'

$s_1(t)=A=\sqrt{2}P,\ Ts/4\leq t\leq Ts/2$ '01'

$s_2(t)=A=\sqrt{2}P,\ Ts/2\leq t\leq 3Ts/4$ '10'

$s_3(t)=A=\sqrt{2}P,\ 3Ts/4\leq t\leq Ts$ '11'

All lasers send the same symbol towards every photodetector (repetition coding). Every photodetector counts the photoelectrons it receives in every QPPM symbol slot. The received symbol of the *n*th photodetector, is a vector of *Q* photoelectron counts $\{\boldsymbol{Z_{nq}};\ q = 1,\ldots\ldots\ldots,Q\}$ and it is passed to the processor and finally decoded to binary data bits. The wavelength chosen for free space optical systems usually falls near one of two wavelengths, 0.85 μm or 1.55 μm. The shorter of the two wavelengths is cheaper and is favored for shorter distances. The eye hazard at 1.55 μm is much lower than at 0.85 μm.

3.3.5 Receiver for Uncoded System

At the receiver the received signal *r(t)* after optical/electrical conversion is:

$$r(t) = \eta h(t)I_0 + n(t)$$

where I_0 =the average transmitted light intensity and

$I = hI_0$ =the corresponding received intensity in an ON PPM slot.

h =the channel fading coefficient

n =receiver noise.

An ideal photon-counting model with a typical quantum efficiency is assumed. Figure 3.6 illustrates the receiver model for the system.

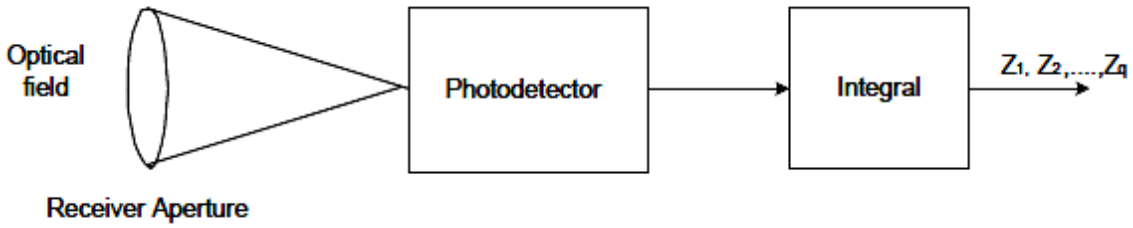

Fig. 3.6: Optical detection model of free-space communication system

3.3.4 System Analysis

The aggregate optical field from all the lasers is detected by each photodetector and we denote the total incident signal power at one photodetector for a non-fading channel from all the lasers as P_r when a pulse is transmitted. Z_{nq} is the number of photoelectrons at slot q collected by photodetector n. Z_{nq} is a Poisson random variable with mean value depending on the receiving power, background power, receiver efficiency and receiver time slot duration. The average number of signal photoelectrons generated in a QPPM slot in which a pulse is transmitted is denoted as

$$\lambda_s = \frac{\eta \mathrm{P}_r T_Q}{hf} \tag{3.3.2}$$

where η is the detector's quantum efficiency factor, defined as the ratio of generated photoelectrons to incident photons, assumed to be 0.5 here. T_Q is the slot duration equal to T_s/Q. h is Planck's constant, and f is the optical center frequency.

In addition to the signal, background radiation is received. The average number of photoelectrons due to the background field is denoted as

$$\lambda_b = \frac{\eta \mathrm{P}_b T_Q}{hf} \tag{3.3.3}$$

where P_b is the incident background power on one photodetector. At the receiver end, in a slot a pulse is sent (what we call an 'on' slot), the photodetector receives both incident power and background noise. The probability mass function for the number of counts in an 'on' slot is

$$\mathrm{P}_r(Z_{nq} = k) = \frac{(\lambda_s + \lambda_b)^k \exp\left(-(\lambda_s + \lambda_b)\right)}{k!}, k = 0,1,2,..... \tag{3.3.4}$$

In the slot where no pulse is sent (what we call an 'off' slot), the photodetector receives only background noise. The probability mass function for the number of counts in an 'off' slot is

$$\mathrm{P}_r(Z_{nq} = k) = \frac{(\lambda_b)^k \exp\left(-(\lambda_b)\right)}{k!}, k = 0,1,2,..... \tag{3.3.5}$$

In the fading case, we denote the path gain from the m^{th} laser to the n^{th} photodetector as a_{nm}. The mean number of the photoelectrons at the n^{th} detector in the signal 'on' slot is derived from

the sum of incident powers from all ***M*** lasers plus background noise; the mean number becomes

$$\lambda_{on} = \frac{\lambda_s}{M} \sum_{m=1}^{M} a_{nm}^2 + \lambda_b \tag{3.3.6}$$

To be fair in our comparisons, we keep the total laser power constrained by assuming the transmit power is equally shared among ***M*** lasers, so P_r is the power received form all M lasers to one photodetector. This parallels the standard assumption for the microwave MIMO system.

We designate the collection of slot-by-slot photoelectron counts for the $\boldsymbol{n}^{\mathbf{th}}$ photodetector at the $\boldsymbol{q}^{\mathbf{th}}$ slot in a symbol as $[Z_{nq}, n = 1,\ldots\ldots,N, q = 1, \ldots\ldots Q]$, where ***n*** describes the photodetector number and ***q*** describes the slot number. Then $Z = [Z_{nq}]$ is the received observation matrix.

Suppose X is the whole set of possible symbols, i.e, every $\boldsymbol{x} \in \boldsymbol{X}$ is a ***Q*** slot symbol with ***w*** slots 'on' and ***(Q-w)*** slots 'off'. For every fading matrix **A** with entries $\boldsymbol{a_{nm}}$, the maximum likelihood detector is given by

$$\hat{x} = \arg \max_{x \in X} f(Z \mid x, A) \tag{3.3.7}$$

Since the Z_{nq} are all independent of each other, the conditional distribution of the N X Q random matrix Z can be written as a ***N X Q***-fold product over all of the individual elements Z_{nq}.

$$\hat{x} = \arg \max_{x \in X} \prod_{n=1}^{N} \prod_{q=1}^{Q} \frac{\exp\left(-\frac{\lambda_s}{M} x_q \sum_{m=1}^{M} a_{nm}^2 + \lambda_b \right) \left(\frac{\lambda_s}{M} x_q \sum_{m=1}^{M} a_{nm}^2 + \lambda_b \right)^{Z_{nq}}}{Z_{nq}!}$$

$$= \arg \max_{x \in X} \prod_{n=1}^{N} \prod_{q=1}^{Q} \exp\left(-\frac{\lambda_s}{M} x_q \sum_{m=1}^{M} a_{nm}^2 + \lambda_b \right) \left(\frac{\lambda_s}{M} x_q \sum_{m=1}^{M} a_{nm}^2 + \lambda_b \right)^{Z_{nq}} \tag{3.3.8}$$

We define the set of the 'on' slots as Q_{on} and the set of all the 'off' slot as Q_{off} . Their sizes are ***w*** and ***Q - w*** respectively. The sets Q_{on} and Q_{off} depend on the symbol ***x***. These elements are conditioned on whether they are in Q_{on}, or in $Q_{of.f}$

$$\hat{x} = \arg \max_{x \in X} \prod_{n=1}^{N} \prod_{q \in Q_{on}} \exp\left(-\frac{\lambda_s}{M} \sum_{m=1}^{M} a_{nm}^2 + \lambda_b \right) \left(\frac{\lambda_s}{M} \sum_{m=1}^{M} a_{nm}^2 + \lambda_b \right)^{Z_{nq}} \prod_{q \in Q_{off}} \exp(-\lambda_b) (\lambda_b)^{Z_{nq}} \tag{3.3.9}$$

which can be rewritten as

$$\hat{x} = \arg \max_{x \in X} \sum_{n=1}^{N} \left(\sum_{q \in Q_{on}} Z_{nq} \log \left(\frac{\lambda_s}{M} \sum_{m=1}^{M} a_{nm}^2 + \lambda_b \right) + \sum_{q \in Q_{off}} Z_{nq} \log(\lambda_b) \right)$$

$$= \arg \max_{x \in X} \sum_{n=1}^{N} \sum_{q \in Q_{on}} Z_{nq} \log \left(\frac{\lambda_s}{M} \sum_{m=1}^{M} a_{nm}^2 + \lambda_b \right) + \sum_{n=1}^{N} \left(\sum_{q \in Q} Z_{nq} \log(\lambda_b) - \sum_{q \in Q_{on}} Z_{nq} \log(\lambda_b) \right)$$

$$= \arg \max_{x \in X} \sum_{n=1}^{N} \sum_{q \in Q_{on}} Z_{nq} \log \frac{\left(\frac{\lambda_s}{M} \sum_{m=1}^{M} a_{nm}^2 + \lambda_b \right)}{\lambda_b} \tag{3.3.10}$$

Therefore, the ML detector would make a decision based on a weighted sum over the 'on'slots. If background noise can be ignored, the ML detector chooses the slots that photons are received and makes a free guess if there are some slots pulses were sent but nothing received. In case there is no channel fading, the ML detector does not need to weight Z_{nq}. The ML detector just compares the sum of the photoelectrons counts of all $\boldsymbol{N}$ photodetector in every slots and chooses the largest $\boldsymbol{w}$ slots. When channel fading and background noise are both present, we propose to use an equal-gain combiner instead of the ML detector since monitoring the channel gains increases the complexity of the receiver and has only a slight benefit. An equal gain combiner simply adds the output of every detector without weighting them. In summary, in all cases we form the sum over all detector counts slot by slot and choose the slots with the largest counts.

$$\hat{x} = \arg \max_{x \in X} \sum_{q \in Q_{on}} \sum_{n=1}^{N} Z_{nq} \tag{3.3.11}$$

3.2.5 Error Probability Analysis for Uncoded System

We consider four cases: without or with background radiation, and non-fading or fading links. We discuss a general theory, and illustrate with specific results for the most interesting cases. The situation without background radiation and non-fading links is the easiest and is treated first. All these cases are discussed for both Lognormal and Gamma-gamma model.

Case:1 No Fading, No Background Radiation

With no loss of generality, we assume the symbol with the first *w* of total *Q* slots 'on' is sent. At the receiver end, we receive a matrix **Z** with elements [$\boldsymbol{Z_{nq}}$, n = 1,…….*N;* q = 1,….. ,*Q*] where *n* indicates the receiver number and ***q*** indicates the slot number. Since there is no background radiation, then λ_b = 0. If slot $\boldsymbol{q \in Qo_{f\,f}}$ $\boldsymbol{Z_{nq}}$ will be zero. The channel gain is the same for all paths with $\boldsymbol{a_{nm}}$ = 1. The maximum likelihood detector becomes

$$\hat{x} = \arg \max_{x \in X} \sum_{n=1}^{N} \sum_{q \in Q_{on}} Z_{nq} \log \frac{\left(\frac{\lambda_s}{M} \sum_{m=1}^{M} a_{nm}^2 + \lambda_b \right)}{\lambda_b}$$

$$= \arg \max_{x \in X} \sum_{n=1}^{N} \sum_{q \in Q_{on}} Z_{nq} \log \left(\frac{\lambda_s + \lambda_b}{\lambda_b} \right)$$

$$= \arg \max_{x \in X} \sum_{q \in Q_{on}} \sum_{n=1}^{N} Z_{nq} \tag{3.3.12}$$

In this case, an error will only occur when one or more of the ***w*** 'on' slots register zero counts at *all N* detector outputs and likelihood ties represents the only mechanism for decision error. When $\boldsymbol{Q = 2}$ and $\boldsymbol{w = 1}$ this is equivalent to a binary erasure channel. Specifically, suppose ***i*** of the ***w*** 'on' slots $\boldsymbol{(i \le w)}$ produce a column of zeros in the Z matrix where non-zero counts are expected. Then, a likelihood tie occurs among $\boldsymbol{Q\text{-}w\text{+}i}$ candidates and tie-breaking errors have probability

$$P\left[making\ an\ error\right] = \frac{\binom{Q-w+i}{i} - 1}{\binom{Q-w+i}{i}} = t\left(Q, w, i\right) \tag{3.3.13}$$

By the Poisson property and independence we have that the probability of exactly ***i*** of ***w*** columns registering zero counts is

$$P\left[i\ of\ w\ columns = 0\right] = \binom{w}{i} p^i \left(1-p\right)^{w-i} \tag{3.3.14}$$

where $p = e^{-\lambda s}$, and $\lambda_s = \acute{}P_r T_Q/hf = \eta P_r T_s/hfQ$ from (3.3.2). Putting this altogether we can derive the symbol error probability in no background radiation, for a non-fading channel

$$P_s = \sum_{i=1}^{w} \binom{w}{l} t(Q,w,i)\, p^i (1-p)^{w-i} \tag{3.3.15}$$

By expanding the last term using a binomial expansion, i.e.

$$(1-p)^{w-i} = \sum_{l=0}^{w-i} (-1)^l \binom{w-i}{l} p^l \tag{3.3.16}$$

we can combine terms to get a finite series expansion for symbol error probability:

$$P_s = \sum_{i=1}^{w} \sum_{l=0}^{w-i} (-1)^l \binom{w}{i} \binom{w-i}{i} t(Q,w,i)\, p^i (1-p)^{w-i} e^{-\lambda_s N (i+l)} \tag{3.3.17}$$

From the equation it is found that, for a fixed total transmitter energy, the probability of symbol error is independent of ***M***, i.e., there is no phased-array gain attached to the multiple sources, since these are non-coherent sources. The effective received power does increase linearly with ***N***, the effect of increasing receiving aperture size.

By the Poisson property and independence, the SEP for both lognormal and gamma-gamma model is given by [1],

$$P_s = \frac{Q-1}{Q} \left[e^{-\frac{M \eta (\frac{P_r}{M}) T_s}{hfQ}} \right]^N = \frac{Q-1}{Q} e^{-\frac{\eta E_s N}{hf}} \tag{3.3.18}$$

since tie-breaking errs with probability(Q-1)/Q . It is convenient to consider the BEP, which for QPPM is given by [1],

$$P_b = \frac{\frac{Q}{2}}{Q-1} P_s = \frac{1}{2} e^{-\frac{\eta E_s N}{hf}} \tag{3.3.19}$$

The equation shows that, for a fixed total symbol transmitter energy, the probability of bit error is independent of M , i.e., there is no phased-array gain attached to the multiple sources, since these are noncoherent sources. The effective received power does increase, however, with N , which can be interpreted as the effect of increasing receiving aperture size, or increasing the optical gain. Moreover, the BEP is independent of ***Q*** for a fixed energy per symbol. However, as ***Q*** increases for a fixed bit rate, the peak power must increase as ***Q/log₂ Q*** to maintain fixed energy per symbol.

Case II: Fading Channel, No Background Radiation

First, we assume the channel gain of every laser-detector pair is fixed over a symbol duration. Letting a_{mn} denote the amplitude fading on the path from laser m to photodetector n, we define the channel gain matrix as A with element [a_{nm}, n =1,……,N, m = 1, ……M]. The probability of symbol error conditioned on the fading variables is

$$P_{s|A} = \sum_{i=1}^{w} \sum_{l=0}^{w-i} (-1)^l \binom{w}{i} \binom{w-i}{i} t(Q,w,i) e^{-\frac{\lambda_s}{M} \sum_n \sum_m a_{nm}^2 (i+l)} \tag{3.3.20}$$

To extend the analysis of non-fading link and no background radiation case to the case of link fading, we can simply average the (conditional) symbol error probability of (3.3.20), with respect to the joint fading distribution of the A_{nm} variables. We emphasize that this produces the symbol error probability averaged over fades. Formally, we find P_s by evaluating

$$P_S = \int P_{s|A} f_A(a) da \tag{3.3.21}$$

where the integral is interpreted as an MN-dimensional integral. Since the A_{nm} variables are assumed independent, the above averaging leads to

$$P_s = \sum_{i=1}^{w} \sum_{l=0}^{w-i} (-1)^l \binom{w}{i} \binom{w-i}{i} t(Q,w,i) \left(\int_0^{\infty} e^{-\frac{\lambda_s}{M}(i+l)a^2} f_A(a) da \right)^{MN} \tag{3.3.22}$$

If the channel is under log-normal fading, we can at least evaluate (3.3.22) numerically.

The probability of zero count in slot 1 at detector n is given by [1],

$$P\left[Z_{n1} = 0 \mid slot1, A\right] = e^{-\sum_{m=1}^{M} a_{nm}^2 \left(\frac{\eta P_r}{Mhf}\right)\left(\frac{T_s}{Q}\right)} \tag{3.3.23}$$

$$P\left[allZ_{n1} = 0 \mid slot1, A\right] = e^{-\sum_{m=1}^{M} \sum_{n=1}^{n} a_{nm}^2 \left(\frac{\eta P_r}{Mhf}\right)\left(\frac{T_s}{Q}\right)} \tag{3.3.24}$$

If the path gains are independently distributed and identical, the average symbol error is given by [1],

$$P_s = \int P_{s|A} f_A(a) da = \frac{Q-1}{Q} \left\{ \left[\int e^{-\frac{a^2 \eta \left(\frac{E_s}{M} \right)}{hf}} f_A(a) da \right]^N \right\}^M \tag{3.3.25}$$

$$f_A(a) = \frac{1}{(2\pi\sigma_x^2)^{\frac{1}{2}} a} \exp\left(-\frac{(\log_e a - \mu_x)^2}{2\sigma_x^2}\right), \tag{3.3.26}$$

In case of gamma-gamma fading, we can at least evaluate (3.3.22) numerically.
The probability of zero count in slot 1 at detector n is

$$P\left[Z_{n1} = 0 \mid slot1, A\right] = e^{-\sum_{m=1}^{M} a_{nm}^2 \left(\frac{\eta P_r}{Mhf} \right) \left(\frac{T_s}{Q} \right)} \tag{3.3.27}$$

$$P\left[allZ_{n1} = 0 \mid slot1, A\right] = e^{-\sum_{m=1}^{M} \sum_{n=1}^{n} a_{nm}^2 \left(\frac{\eta P_r}{Mhf} \right) \left(\frac{T_s}{Q} \right)} \tag{3.3.28}$$

If the path gains are independently distributed and identical, the average symbol error becomes

$$P_s = \int P_{s|A} f(I) dI = \frac{Q-1}{Q} \left\{ \left[\int e^{-\frac{a^2 \eta \left(\frac{E_s}{M} \right)}{hf}} f(I) dI \right]^N \right\}^M \tag{3.3.29}$$

$$f(I) = \frac{2(\alpha\beta)^{(\alpha+\beta)/2}}{\Gamma(\alpha)\Gamma(\beta)} I^{\frac{(\alpha+\beta)}{2}-1} K_{(\alpha-\beta)}(2\sqrt{\alpha\beta I}), I > 0 \tag{3.3.30}$$

I is the signal intensity $\Gamma(.)$ is the gamma function, and $K_{(\alpha-\beta)}$ is the modified Bessel function of the second kind and order $(\alpha-\beta)$.α and β are p.d.f parameters describing the scintillation experienced by plane waves, and in the case of zero-inner scale.
Converting to BEP

$$P_b = \frac{1}{2} \left[\int_0^{\infty} P_{S|A} f(z) dz \right]^{M N} \tag{3.3.31}$$

where f(z)= lognormal or gamma-gamma p.d.fs.

Case III: No Channel Fading, with Background Radiation

At the receiver end, it received a matrix **Z** with elements [Z_{nq}, n = 1,…….,N, q =1,……..,Q]. $\boldsymbol{\lambda_b}$ is the Poisson count random variable parameter due to the background radiation, and if slot $\boldsymbol{q}$ is an 'off' slot, $\boldsymbol{Z_{nq}}$ will be also a Poisson distributed random variable with parameter λ_b. For signal 'on' slot, the Poisson count random variable parameter is $\lambda_s+\lambda_b$. The channel gain is the same for all paths with $\boldsymbol{a_{nm}}$ = 1.

Again, we assume without lose of generality that the symbol with the first $\boldsymbol{w}$ slot 'on' is send. The maximum likelihood detector becomes

$$\begin{aligned} \hat{x} &= \arg \max_{x \in X} \sum_{n=1}^{N} \sum_{q \in Q_{on}} Z_{nq} \log\left(\frac{\lambda_s}{M} \sum_{m=1}^{M} a^2 + \lambda_b \right) \\ &= \arg \max_{x \in X} \sum_{q \in Q_{on}} \sum_{n=1}^{N} Z_{nq} \end{aligned} \tag{3.3.32}$$

where $\boldsymbol{Q_{on}}$ = [1,…….,w] is the set of all 'on' slot that pulses are sent and $\boldsymbol{Q_{off}}$ = [w + 1, ……,Q] is the set of all 'off' slot that only background noise is received. Detection is correct only if all of the noise slot counts $\boldsymbol{Z_{nq}}$ are less than all the signal slot counts. Thus the symbol error probability is given by

$$P_s \leq 1\text{-}P(\text{all signal slot counts greater than noise slot counts}) \tag{3.3.33}$$

Adding the tie-break part, we can get the exact error probability.

$$\begin{aligned} P_s \leq\ & P\left[\min(Z_{on}) < \max(Z_{off}) \right] \\ =\ & 1 - \sum_{i=1}^{\infty} \left(poisson\ \ pmf\ \ \left(N(\lambda_s + \lambda_b), i+1 \right) \right) \\ & X\ \left(1 - \left(poisson\ \ cmf\ \ \left(N(\lambda_s + \lambda_b), i \right) \right) \right)^{w-1} \\ & X\ \left(poisson\ \ cmf\ \ \left(N(\lambda_b), i \right) \right)^{Q-w-1} \end{aligned} \tag{3.3.34}$$

where *Poissonpmf*(*x*,*y*) represent the Poisson p.d.f at value ***y*** using the corresponding parameter ***x*** and *Poissoncmf*(*x*,*y*) represent the Poisson probability cumulative function at value ***y*** using the corresponding parameter ***x***.

For the exact error probability

$$P_s = P\left[\min(Z_{on}) < \max(Z_{off})\right] + \sum_{k=1}^{w}\sum_{s=1}^{Q-w}\binom{k+s}{s} P\left[\min(\underline{Z_{on}}) = \max(\underline{Z_{off}})\right] \tag{3.3.35}$$

we can get a precise form

$$P_s = P\left[\min(Z_{on}) < \max(Z_{off})\right] + \sum_{k=1}^{w}\sum_{s=1}^{Q-w}\binom{k+s}{s} P\left[\min(\underline{Z_{on}}) = \max(\underline{Z_{off}})\right] \tag{3.3.36}$$

where ***s*** minimal signal slots have the same counts as ***k*** maximum noise slots.

Then the exact error probability can be written for both lognormal and Gamma-gamma channel as

$$P_s \leq 1 - P\left[all\ Z_q < Z_1\right] = 1 - \left(P\left[Z_2 < Z_1\right]\right)^{Q=1} = 1 - \left[\sum_{i=1}^{\infty}\sum_{j=0}^{i-1} P\left(Z_1 = i, Z_2 = j\right)\right]^{Q-1} \tag{3.3.37}$$

A union bound on symbol error probability will be dominated by error events with symbol Hamming distance 2, of which there are ***w(Q- w)*** occurrences.

$$P_s \approx w(Q-w)P[dis\tan ce - 2error] \tag{3.3.38}$$

The latter two-signal probability can be bounded, using the appropriate Poisson distributions, by a Chernoff bound

$$P[dis\tan ce - 2error] \leq \frac{\exp\left(2\lambda_b\left(\left(1+\mu\right)^{\frac{1}{2}} - 1\right) - \lambda_s\right)}{2} \tag{3.3.39}$$

where $\mu = \frac{n_s}{n_b}$. Expanding the exponent with a Taylor series in μ for small μ gives

$$P_S \approx \frac{w(Q-w)}{2}\exp\left(-\frac{\lambda_S^2}{4\lambda_B}\right) \tag{3.3.40}$$

Case IV: Fading Channel, with Background Radiation

This case is the most general in practice, and there is no simple expression for the symbol error probability. Here some incorrect symbol can have higher likelihood (an incorrect set of ***w*** slots have larger weighted column sums) same as in Case III. By using equal-gain-combiner, the upper bound on $\boldsymbol{P_s}$ conditioned on fading path gain matrix A is

$$P_s \le 1 - \sum_{i=1}^{\infty} \left(poisson\ pmf\ \left(\sum_{n=1}^{N}\sum_{m=1}^{M} a_{nm}^2 \frac{\lambda_s}{M} + N\lambda_b, i+1 \right) \right) X \left(1 - \left(poisson\ cmf\ \left(\sum_{n=1}^{N}\sum_{m=1}^{M} a_{nm}^2 \frac{\lambda_s}{M} + N\lambda_b, i+1 \right) \right) \right)^{w-1} X \left(poisson\ cmf\ \left(N(\lambda_b), i-1 \right) \right)^{Q-w-1} \quad (3.3.41)$$

We can get the overall symbol error probability by averaging the conditional symbol error probability. Numerical integration is a prohibitively slow process due to the large number of fading variables combined with the infinite summation. In this case, using numerical integration is not an efficient way to calculate the symbol error probability. We use simulation instead to analyze the performance of the MIMO system.

For both log-normal and gamma-gamma case, the optimal detector is as described by the following equation. We propose instead a more realistic design of simply summing over the received PD counts for each time slot as was optimal for the cases presented above. Channel estimation at the receiver is thereby avoided in exchange for a small performance penalty.

$$P_{S/X} = 1 - \left[\sum_{i=1}^{\infty} \sum_{j=0}^{i-1} \frac{\left(N(\lambda_s + \lambda_b) \right)^i e^{-N(\lambda_s+\lambda_b)}}{i!} X \frac{\left(N\lambda_b \right) j e^{-N\lambda_b}}{j!} \right]^{Q-1} \quad (3.3.42)$$

The average symbol error becomes

$$P_s = \int P_{S|X}\ f(z)\, dz \quad (3.3.43)$$

where f(z)= lognormal or gamma-gamma p.d.fs.

3.4 Basis of LDPC Code

Low-density parity-check (LDPC) codes are a class of linear block codes. The name comes from the characteristic of their parity-check matrix which contains only a few 1's in comparison to the numberof 0's. Their main advantage is that they provide a performance which is very close to the capacity for a lot of different channels and linear time complex algorithms for decoding. Furthermore are they suited for implementations that make heavy use of parallelism.

They were first introduced by Gallager in his PhD thesis in 1960. But due to the computational effort in implementing coder and en- coder for such codes and the introduction of Reed-Solomon codes, they were mostly ignored until about ten years ago.

3.4.1 Representations of LDPC Codes

Basically there are two different possibilities to represent LDPC codes. Like all linear block codes they can be described via matrices. The second possibility is a graphical representation.

Matrix Representation

Lets look at an example for a low-density parity-check matrix first.The matrix defined in equation (3.4.1) is a parity check matrix with dimension n ×m for a (8, 4) code. We can now define two numbers describing these matrix. w_r for the number of 1's in each row and w_c for the columns. For a matrix to be called low-density the two conditions $w_c << n$ and $w_r << m$ must be satisfied. In order to do this, the parity check matrix should usually be very large, so the example matrix can't be really called low-density.

$$H = \begin{bmatrix} 0 & 1 & 0 & 1 & 1 & 0 & 0 & 1 \\ 1 & 1 & 1 & 0 & 0 & 1 & 0 & 0 \\ 0 & 0 & 1 & 0 & 0 & 1 & 1 & 1 \\ 1 & 0 & 0 & 1 & 1 & 0 & 1 & 0 \end{bmatrix} \tag{3.4.1}$$

Graphical Representation

Tanner introduced an effective graphical representation for LDPC codes. Fig. 3.7 is an example for such a Tanner graph and represents the same code as the matrix in 3.1. The creation of such a graph is rather straight forward. It consists of **m** check nodes (the number of parity bits) and **n** variable nodes (the number of bits in a codeword). Check node $\mathbf{f_i}$ is connected to variable node $\mathbf{c_j}$ if the element $\mathbf{h_{ij}}$ of **H** is a 1.

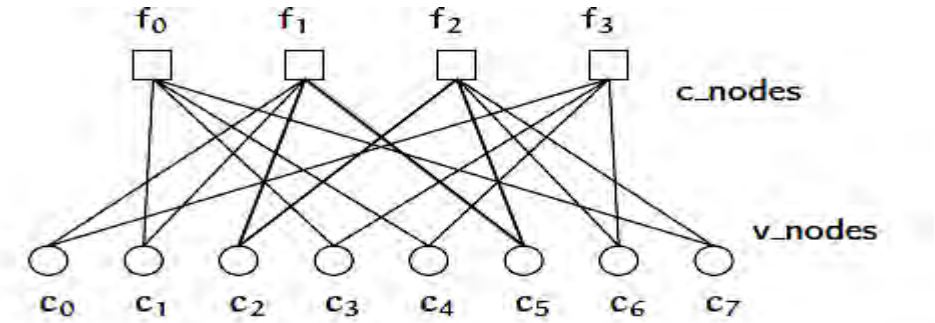

Fig. 3.7: Tanner graph corresponding to the parity check matrix in equation (3.4.1) The marked path $c_2 \rightarrow f_1 \rightarrow c_5 \rightarrow f_2 \rightarrow c_2$ is an example for a short cycle. Those should usually be avoided since they are bad for decoding performance.

3.4.2 Design of LDPC Codes

Several different algorithms exists to construct suitable LDPC codes. Gallager himself introduced one. Furthermore MacKay proposed one to semi-randomly generate sparse parity check matrices. This is quite interesting since it indicates that constructing good performing LDPC codes is not a hard problem. In fact, completely randomly chosen codes are good with a high probability. The problem that will arise, is that the encoding complexity of such codes is usually rather high. So the design contents are

- Large dmin
- No short cycles

- Cycles exist in Tanner graphs.

-The shortest possible cycle has the length 4.

- Although we can eliminate all cycles with length 4, we may still have cycles with length 6.

- No eliminating sets

- Applications in binary erasure channels.

3.4.3 Encoding of LDPC Codes

The code word would consist of the message bits and some parity check bits. So far nowhere was mentioned that it's possible to directly see the original message bits in a LDPC encoded message. Luckily it is. Encoding LDPC codes is roughly done like that: Choose certain variable nodes to place the message bits on. And in the second step calculate the missing values of the other nodes. An obvious solution for that would be to solve the parity check equations. This would contain operations involving the whole parity-check matrix and the complexity would be again quadratic in the block length. In practice however, more clever methods are used to ensure that encoding can be done in much shorter time. Those methods can use again the spareness of the parity-check matrix or dictate a certain structure3 for the Tanner graph.

3.4.4 Decoding of LDPC Codes

The algorithm used to decode LDPC codes was discovered independently several times and as a matter of fact comes under different names. The most common ones are the belief propagation algorithm, the message passing algorithm and the sum-product algorithm. In order to explain this algorithm, a very simple variant which works with hard decision, will be introduced first. Later on the algorithm will be extended to work with soft decision which generally leads to better decoding results. Only binary symmetric channels will be considered.

◊ Hard Decision Decoding

The algorithm will be explained on the basis of the example code already introduced in equation 3.3.1 and Fig. 3.6. An error free received codeword would be e.g. c = [1 0 0 1 0 1 0 1]. Let's suppose that we have a BHC channel and the received the codeword with one error – bit c_1 flipped to 1.

1. In the first step all v-nodes c_i send a "message" to their (always2 in our example) c-nodes f_j containing the bit they believe to be the correct one for them. At this stage the only information a v-node c_i has, is the corresponding received i-th bit of c, y_i. That means for example, that c_0 sends a message containing 1 to f_1 and f_3, node c_1 sends messages containing y_1 (1) to f_2 and f_1, and so on.

Table 3.1: overview over messages received and sent by the c-nodes in step 2 of the message passing algorithm

C-node	received/sent				
f_0	Received:	$c_1 \rightarrow 1$	$c_3 \rightarrow 1$	$c_4 \rightarrow 0$	$c_7 \rightarrow 1$
	Sent:	$0 \rightarrow c_1$	$0 \rightarrow c_3$	$1 \rightarrow c_4$	$0 \rightarrow c_7$
f_1	Received:	$c_0 \rightarrow 1$	$c_1 \rightarrow 1$	$c_2 \rightarrow 0$	$c_5 \rightarrow 1$
	Sent:	$0 \rightarrow c_0$	$0 \rightarrow c_1$	$1 \rightarrow c_2$	$0 \rightarrow c_5$
f_2	Received:	$c_2 \rightarrow 0$	$c_5 \rightarrow 1$	$c_6 \rightarrow 0$	$c_7 \rightarrow 1$
	Sent:	$0 \rightarrow c_2$	$1 \rightarrow c_5$	$0 \rightarrow c_6$	$1 \rightarrow c_7$
f_3	Received:	$c_0 \rightarrow 1$	$c_3 \rightarrow 1$	$c_4 \rightarrow 0$	$c_6 \rightarrow 0$
	Sent:	$1 \rightarrow c_0$	$1 \rightarrow c_3$	$0 \rightarrow c_4$	$0 \rightarrow c_6$

2. In the second step every check nodes f_j calculate a response to every connected variable node. The response message contains the bit that f_j believes to be the correct one for this v-node c_i assuming that the other v-nodes connected to f_j are correct

3. Next phase: the v-nodes receive the messages from the check nodes and use this additional information to decide if their originally received bit is OK. Table 3.2 illustrates this step. Now the v-nodes can send another message with their (hard) decision for the correct value to the check nodes.

Table 3.2: Step 3 of the described decoding algorithm. The v-nodes use the answer messages.

v-node	y_i received	message from check nodes		Decision
C_0	1	$f_1 \rightarrow 0$	$f_3 \rightarrow 1$	1
C_1	1	$f_0 \rightarrow 0$	$f_1 \rightarrow 0$	0
C_2	0	$f_1 \rightarrow 1$	$f_2 \rightarrow 0$	0
C_3	1	$f_0 \rightarrow 0$	$f_3 \rightarrow 1$	1
C_4	0	$f_0 \rightarrow 0$	$f_3 \rightarrow 0$	0
C_5	1	$f_1 \rightarrow 0$	$f_2 \rightarrow 1$	1
C_6	0	$f_2 \rightarrow 0$	$f_3 \rightarrow 0$	0
C_7	1	$f_0 \rightarrow 1$	$f_2 \rightarrow 1$	1

◊Soft Decision Decoding

Soft-decision decoding of LDPC codes, which is based on the concept of belief propagation, yields in a better decoding performance than the hard decision decoding and is therefore the preferred method. The underlying idea is exactly the same as in hard decision decoding. Before presenting the algorithm lets introduce some notations:

• $P_i = P_r(c_i = 1|y_i)$

• q_{ij} is a message sent by the variable node ci to the check node fj. Every message contains always the pair $q_{ij}(0)$ and $q_{ij}(1)$ which stands for the amount of belief that yi is a ”0” or a ”1”.

• rji is a message sent by the check node f_j to the variable node c_i. Again there is a $r_{ji}(0)$ and $r_{ji}(1)$ that indicates the (current) amount of believe in that y_i is a “0” or a “1”. The step numbers in the following description correspond to the hard decision case.

1. All variable nodes send their $\mathbf{q_{ij}}$ messages. Since no other information is available at this step, $\mathbf{q_{ij}(1) = P_i}$ and $\mathbf{q_{ij}(0) = 1 - P_i}$.

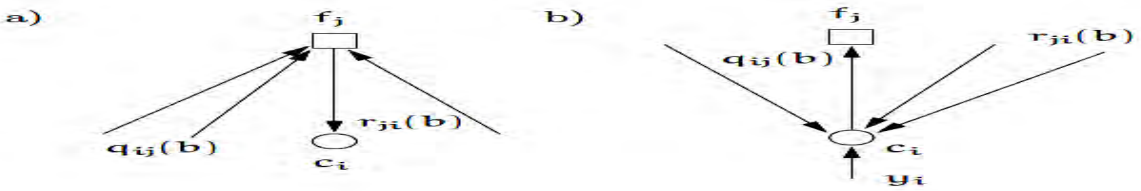

Fig.3.8: a) illustrates the calculation of $r_{ji}(b)$ and b) $q_{ij}(b)$

2. The check nodes calculate their response messages $\mathbf{r_{ji}}^2$

$$r_{ji}(0) = \frac{1}{2} + \frac{1}{2} \prod_{i' \in V_j \setminus i} (1 - 2q_{i'j}(1)) \tag{3.4.2}$$

$$r_{ji}(1) = 1 - r_{ji}(0) \tag{3.4.3}$$

So they calculate the probability that there is an even number of 1’s amoung the variable nodes except $\mathbf{c_i}$ (this is exactly what $\mathbf{V_{ji}}$ means). This probability is equal to the probability $\mathbf{r_{ji}(0)}$ that $\mathbf{c_i}$ is a 0. This step and the information used to calculate the responses is illustrated in Fig.3.8.

3. The variable nodes update their response messages to the check nodes. This is done according to the following equations,

$$q_{ij}(0) = K_{ij}(1-P_i)\prod_{i'\in C_i\setminus j} r_{j'i}(0) \tag{3.4.4}$$

$$q_{ij}(1) = K_{ij}P_i\prod_{j'\in C_i\setminus j} r_{j'i}(1) \tag{3.4.5}$$

whereby the constants K_{ij} are chosen in a way to ensure that $q_{ij}(0)+q_{ij}(1) = 1$. $C_{i\setminus j}$ now means all check nodes except f_j. Again Fig.3.8 illustrates the calculation in this step. At this point the v-nodes also update their current estimation $\hat{c}_i$ of their variable c_i. This is done by calculating the propabilities for 0 and 1 and voting for the bigger one. The used equations

$$Q_i(0) = K_i(1-P_i)\prod_{j'\in C_i} r_{ji}(0) \tag{3.4.6}$$

$$Q_i(1) = K_iP_i\prod_{j'\in C_i} r_{ji}(1) \tag{3.4.7}$$

are quite similar to the ones to compute $q_{ij}(b)$ but now the information from every c-node is used.

$$\hat{c} = \begin{cases} 1 \ if\ Q_i(1) > Q_i(0). \\ 0 \ else \end{cases} \tag{3.4.8}$$

If the current estimated codeword fufills now the parity check equations the algorithm terminates. Otherwise termination is ensured through a maximum number of iterations. The explained soft decision decoding algorithm is a very simple variant, suited for BSC channels and could be modified for performance improvements. Beside performance issues there are numerical stability problems due to the many multiplications of probabilities. The results will come very close to zero for large block lenghts. To prevent this, it is possible to change into the log-domain and doing additions instead of multiplications. The result is a more stable algorithm that even has performance advantages since additions are less costly.

3.5. Performancce Analysis of an LDPC Coded FSO Communication System:

3.5.1 System Model

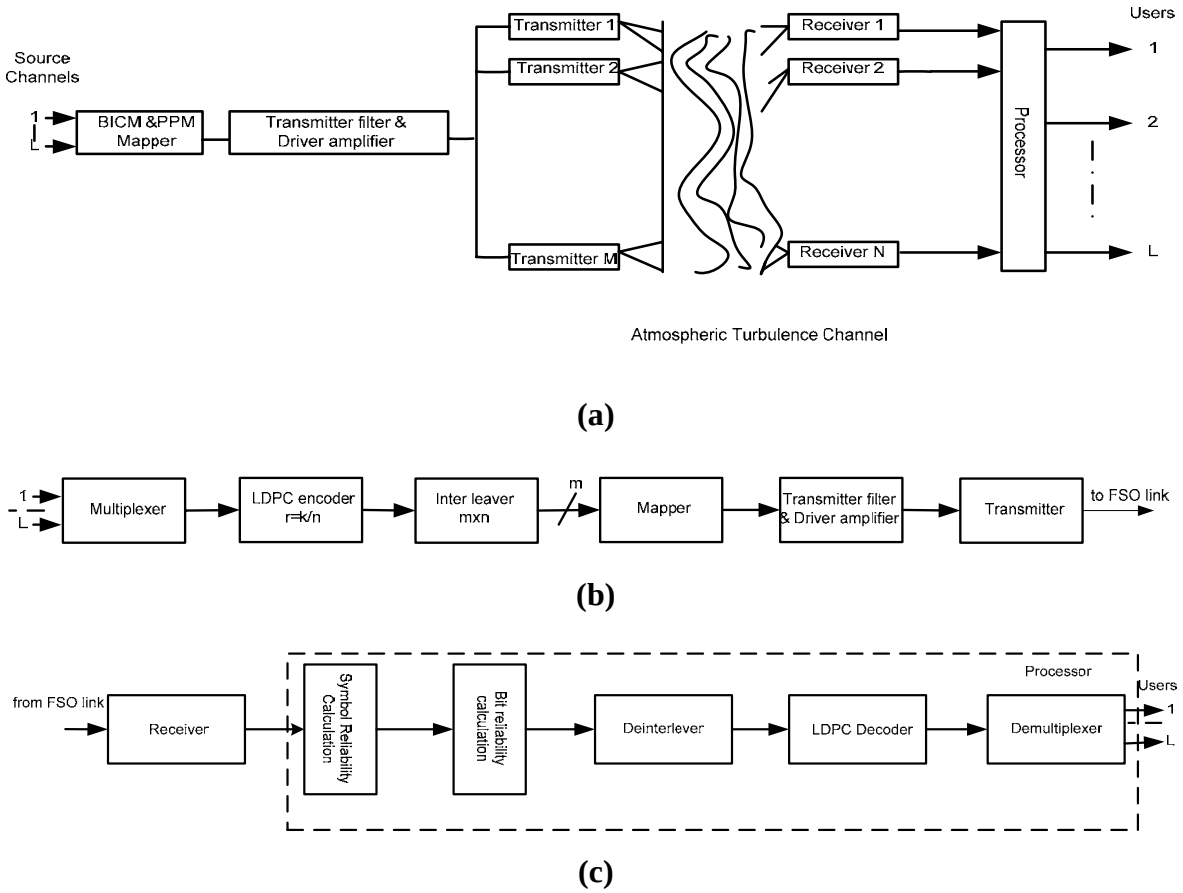

Fig.3.9: (a) Atmospheric optical MIMO system with Q-ary PPM and BICM, (b) transmitter side and (c) processor configuration

Block diagram of the proposed coded-modulation MIMO Q-ary PPM FSO communication system is given in Fig. 3.9(a). The encoder and decoder configurations are given in Fig. 3.9(b) and 3.9(c), respectively. To enable the transmission under the strong atmospheric turbulence we propose the use of the *multi-laser multi-detector* (MLMD) concept .

Although the MLMD concept is analogous to multiple-input multiple-output (MIMO) wireless concept, the underlying physics is different, and both optimal and sub-optimal FSO configurations are required.

3.5.2 Q-ary Pulse Position Modulation

A Q-ary PPM scheme transmits $L=\log_2 Q$ bits per symbol, providing high power efficiency. The source bit streams coming from L sources $\mathbf{u}_i$ (i=1,2,….L) are encoded using $L(n,k_i)$ LDPC encoders of rate $R_i=k_i/n$ where n is the codeword length and k_i is the dimension (information word length) of the i^{th} component LDPC code. The mxn block-interleaver, collects m code-words written row-wise. The mapper accepts m bits at a time from the interleaver column-wise and determines the corresponding slot for **Q**-ary ($Q=2^m$) PPM signaling using a *Gray mapping* rule. With this BICM scheme, the neighboring information bits from the same source are allocated into different PPM symbols. In each signaling interval T_s a pulse of light of duration $T=T_s/Q$ is transmitted by a laser. The signaling interval T_s is subdivided into Q slots of duration T. The total transmitted power P_{tot} is fixed and independent of the number of lasers so that emitted power per laser is P_{tot}/M**.** This technique improves the tolerance to atmospheric turbulence, because different Q-ary PPM symbols experience different atmospheric turbulence conditions The i^{th} (i=1,2,…,M) laser modulated beam is projected toward the j^{th} (j=1,2,…,N) receiver using the expanding telescope, and the receiver is implemented based on a p.i.n. photo detector in a trans-impedance amplifier (TA) configuration. The use of only one LDPC code allows iterating between the *a posteriori* probability (APP) demapper and the LDPC decoder (we will call this step the *outer iteration*), further improving the BER performance.

3.4.3 Transmitter and Receiver for Coded System

We assume that the pulses transmitted are rectangular and of duration

$$T=\log_2 C/(QR_b) \tag{3.5.1}$$

The lasers are aimed at a bank of N photodetectors (PD) .The signal from laser m to photodetector n passes through turbulent atmosphere causing a field gain of A_{nm} on the signal, constant over the duration of transmission. We assume that the photodetectors are placed sufficiently far apart so that the fading parameters can be assumed independent. We also assume the delay spread is so short as to make the fading frequency nonselective.

The photodetectors act as ideal photon counters over each time slot interval. Perfect synchronization is imperative and assumed. The statistic collected by photodetector $\boldsymbol{n}$ over time slot $\boldsymbol{q}$ is an integer denoted $\boldsymbol{Z_{nq}}$, and is assumed to be conditionally Poisson distributed with parameter $\boldsymbol{\lambda_{nq}^{(i)}}$ depending on the codeword matrix sent $\mathbf{x}(i)$ and the fading parameters, with

$$\lambda_{nq}^{(i)} = c\sum_{m=1}^{M} x_{mq}^{(i)} A_{nm}^2 + \lambda_b \tag{3.5.2}$$

where $\boldsymbol{x^{(i)}_{mq}}$ in the $\boldsymbol{mq}$-element of the codeword matrix, and $\boldsymbol{\lambda_b}$ is background radiation also incident on the photodetector. The constant $\boldsymbol{c}$ absorbs the transmit power, average space loss, and responsivity of the photodetector into a single constant,

$$c = \frac{\eta E_s}{hfM} \tag{3.5.3}$$

where $\boldsymbol{\eta}$ is the quantum efficiency of the photodetector, $\boldsymbol{E_s}$ is the average received symbol energy from all lasers over one slot of duration $\boldsymbol{T}$, $\boldsymbol{h}$ is Planck's constant, and $\boldsymbol{f}$ is the laser carrier frequency. Note that in our results the total transmit energy is fixed so that increasing the number of lasers can only provide additional diversity, and not additional energy. Under these assumptions, the maximum likelihood receiver given the fading parameters is given by

$$\hat{i} = \arg \max_{i\in\{1,.....C\}} \sum_{n=1}^{N}\sum_{q=1}^{Q}\left[Z_{nq} \ln\left(\lambda_{nq}^{(i)}\right) - \left(\lambda_{nq}^{(i)}\right)\right] \tag{3.5.4}$$

We are especially interested in balanced codes which have the same row of Hamming weight over all transmitters. In this case, the additive $-\lambda_{\mathrm{nq}}^{(\mathrm{i})}$ term can be dropped from (3.5.4).

The code used by the optical MIMO system must at least be able to operate in an environment with minimal fading. By looking explicitly at this case, i.e., setting $\boldsymbol{A_{nm}} = 1$ almost surely, we can derive some necessary conditions for code design.

We calculate the two-codeword error probability, i.e., the probability that codeword $\mathbf{x}^{(1)}$ is sent but codeword $\mathbf{x}^{(2)}$ is chosen. Note that in the non-fading case, the parameters of the Poisson statistics are equal over the N photodetectors and the sufficient statistic becomes with parameter $\lambda^{(i)}q = N\lambda(i)$. Assuming that ties in (3.5.4) always result in wrong decisions, the two-codeword error probability can be bounded.

The number of photoelectrons in the $\mathbf{q^{th}}$ slot of nth PD, in which a pulse is sent, denoted as $\mathbf{Z_{nq}}$, has a Poisson count distribution [2] with the mean parameter $\mathbf{(\lambda s/M)\Sigma I_{nm}+\lambda_b.I_{nm}}$ is the intensity of the light incident to $\mathbf{n^{th}}$ PD, originated from $\mathbf{m^{th}}$ laser source. The slot without a pulse has a Poisson distribution with mean parameter $\boldsymbol{\lambda_b}$. The PD analysis is based on a semiclassical treatment of the photodetection process as explained in [2]. $\boldsymbol{\lambda_s}$ corresponds to the PD effective number of photoelectrons per slot (per one PD) in the absence of turbulence and background light [2]

$$\lambda_s = \frac{\eta \mathrm{P}_r T_Q}{hf} \tag{3.5.5}$$

while $\boldsymbol{\lambda_b}$ corresponds to the effective number of photoelectrons due to background light

$$\lambda_b = \frac{\eta \mathrm{P}_b T_Q}{hf} \tag{3.5.6}$$

where P_b is the PD incident background noise power,η is the photodiode efficiency, set in simulations to 0.5, h is the Plank constant, is the speed of the light in vacuum, and is the wavelength, set in simulations to 1550 nm. The influence of the atmospheric turbulence channel is described by the gamma–gamma p.d.fs in Eq.3.2.6.

3.5.4 Error Probability Analysis for Coded System

The outputs of the N receivers in response to symbol q, denoted as $\boldsymbol{Z_{nq}}$ (n=1,2,…,N; q=1,2,…,Q), are processed to determine the symbol reliabilities $\boldsymbol{\lambda(q)}$ (q=1,2,…,Q) given by[8]

$$\lambda(q) = -\frac{\sum_{n=1}^{N}\left(Z_{nq} - \frac{\sqrt{E_s}}{M}\sum_{m=1}^{M} I_{n,m}\right)^2}{\sigma^2} - \frac{\sum_{n=1}^{N}\sum_{1\neq q}^{Q} Z_{n,I}}{\sigma^2} \tag{3.5.7}$$

where $\boldsymbol{E_s}$ is the symbol energy of uncoded symbol in electrical domain (in the absence of scintillation), which is related to the bit energy $\boldsymbol{E_b}$ by $\boldsymbol{E_s=E_b log_2 Q}$. $\boldsymbol{\sigma^2}$ is the variance of TA thermal noise (that is modeled as additive white Gaussian noise (AWGN)), and it is related to the double-side power spectral density N_0 by $\boldsymbol{\sigma^2=N_0/2.}$ With $\boldsymbol{I_{nm}}$ we denoted the intensity of the light incident to $\boldsymbol{n^{th}}$ photodetector (n=1,2,…,N), originated from $\boldsymbol{m^{th}}$ (m=1,2,…,M) laser source, which is described by the gamma-gamma p.d.f.

The bit reliabilities $\boldsymbol{L(c_j)}$, (j=1,2,…,m) ($\boldsymbol{c_j}$ is the j^{th} bit in observed symbol q binary representation $\boldsymbol{c}$=(c_1,c_2,…,c_m)) are determined from symbol reliabilities as[8],

$$L\left(c_j\right) = \log \frac{\sum_{c:c_j=0} \exp\left[\lambda\left(q\right)\right]}{\sum_{c:c_j=1} \exp\left[\lambda\left(q\right)\right]} \tag{3.5.8}$$

and forwarded to the LDPC decoder.

We assumed equally probable transmission $\mathbf{(Pr(}q\mathbf{)=1/}Q\mathbf{,}\ q\mathbf{=1,..,}Q\mathbf{)}$, the averaging over different symbols will not affect the result. Notice that the ensemble averaging is to be done for different channel conditions $\boldsymbol{(I_n)}$ and for different thermal noise realizations $\boldsymbol{(Z \mid I_n)}$. Under this condition the SEP is given by $\boldsymbol{P(Z_{nq} \mid I_n)}$, is

$$P(Z_{nq} \mid \vdots\!\vdots\!\vdots_n) = \frac{1}{\sigma\sqrt{2\pi}} \exp\left[-\frac{(Z_{nq} - \vdots\!\vdots\!\vdots_n)^2}{2\sigma^2}\right] \tag{3.5.9}$$

The BER of LDPC codes can be expressed as:

$$BER = \sum_{i=d_{\min}}^{d_{\max}} iP(Z_{nq} \mid I_n) \tag{3.5.10}$$

where d_{min} is the minimum Hamming weight of error events, and d_{max} is the maximum Hamming weight of error events, and $P(Z_{nq} \mid I_n)$ is the probability of an error event with Hamming weight i. $P(Z_{nq} \mid I_n)$ decreases fast with increased channel signal-to-noise ratios(SNRs). As a result, the BER of iterative codes can be divided in to three regions. At low SNRs , all of the $P(Z_{nq} \mid I_n)$'s are large, therefore the BER is the summation of all the terms in (3.5.10),all of which drops at about the same rate with increased SNRs. At high SNRs, the entire $P(Z_{nq} \mid I_n)$'s are small, except for P_{dmin}, which drops slower than other terms. Therefore, the minimum distance error event is the dominant error event at high SNRs. The BER at high SNR can be approximated by:

$$BER \approx d_{\min} P_{d_{\min}} \tag{3.5.11}$$

The electrical SNR per bit is given by,

$$\frac{E_b}{N_o} = \frac{E_S P(Z_{nq} \mid \ddot{I}_n)}{\log_2 M \ \sigma^2} \tag{3.5.12}$$

where $\boldsymbol{E_s}$ is the symbol energy of uncoded symbol in electrical domain (in the absence of scintillation), which is related to the bit energy $\boldsymbol{E_b}$ by $\boldsymbol{E_s=E_b log_2 Q}$. $\boldsymbol{\sigma^2}$ is the variance of TA thermal noise (that is modeled as additive white Gaussian noise (AWGN)), and it is related to the double-side power spectral density N_0 by $\boldsymbol{\sigma^2=N_0/2.}$

3.6 Summary

Theoretical analysis on FSO MIMO communication system based on Q-ary Pulse Position Modulation is given in this chapter. The performances results are evaluated in terms of symbol error rate (SEP) and bit error rate (BER) with several combinations of system parameters for both uncoded and energy efficient bit interleaved LDPC coded modulation scheme.

Chapter 4

Results and Discussion

Results and Discussion

4.1 Introduction

The analytical results are presented and discussed in this chapter. The bit error rate (BER) performances under uncoded and coded condition are calculated as functions of the relevant receiver and input parameter for Q-ary PPM schemes. Also the coding gains have been presented in details for different combination of transmitters and receivers.

4.2 Results and Discussion

Following the analytical approach, we evaluate the performance of uncoded and power efficient coded-modulation scheme based on bit interleaved coded modulation (BICM) with LDPC codes as component codes, suitable for the use in MIMO FSO systems with Q-ary PPM. The coded modulation scheme allows aggregation of RF/microwave signals and a conversion to the optical domain in a very natural way and may be a good candidate for hybrid RF/microwave-FSO systems. The bit-error rate (BER) performance results are evaluated with and without LDPC code in the presence of background radiation.

First the bit error rate performances have been calculated for different number of transmitters and receivers under uncoded and LDPC coded system. We evaluate the bit error rate performance result of a MIMO FSO link with Q-ary PPM and direct detection scheme. The simulations are performed for up to 25 iterations in LDPC decoder, the

influence of scintillation is modeled assuming a lognormal and Gamma-gamma distribution, and an ideal photon counting receiver is employed. The gamma–gamma distribution fits even better than the log-normal distribution in the weak turbulence regime. It will be shown that if we increase the number of transmitters and receivers the performance of the system improves significantly.

For the convenience of the readers the parameters used for computation in this chapter are shown in table 4.1.

Table 4.1: Nominal Parameters of FSO Communication link

Parameter Name	**Value**
Bit Rate, B_r	100 Mbps
Modulation	Q-PPM
Order of PPM, Q	2, 4, 8, ……..
Channel Type	Log-normal, Gamma-gamma
Scintillation Index, S.I.	0.2-3.0
Symbol energy with background noise	-170dBJ
Rytov Variance, σ_x	0.1-0.8
Symbol Energy, E_s	10^{-16} Joules
Quantum efficiency, η	0.5
Operating wavelength, λ	1.55μm

4.3 Performance Analysis of an Uncoded System with Q-ary PPM

4.3.1 Numerical Result and Discussion for Lognormal Channel

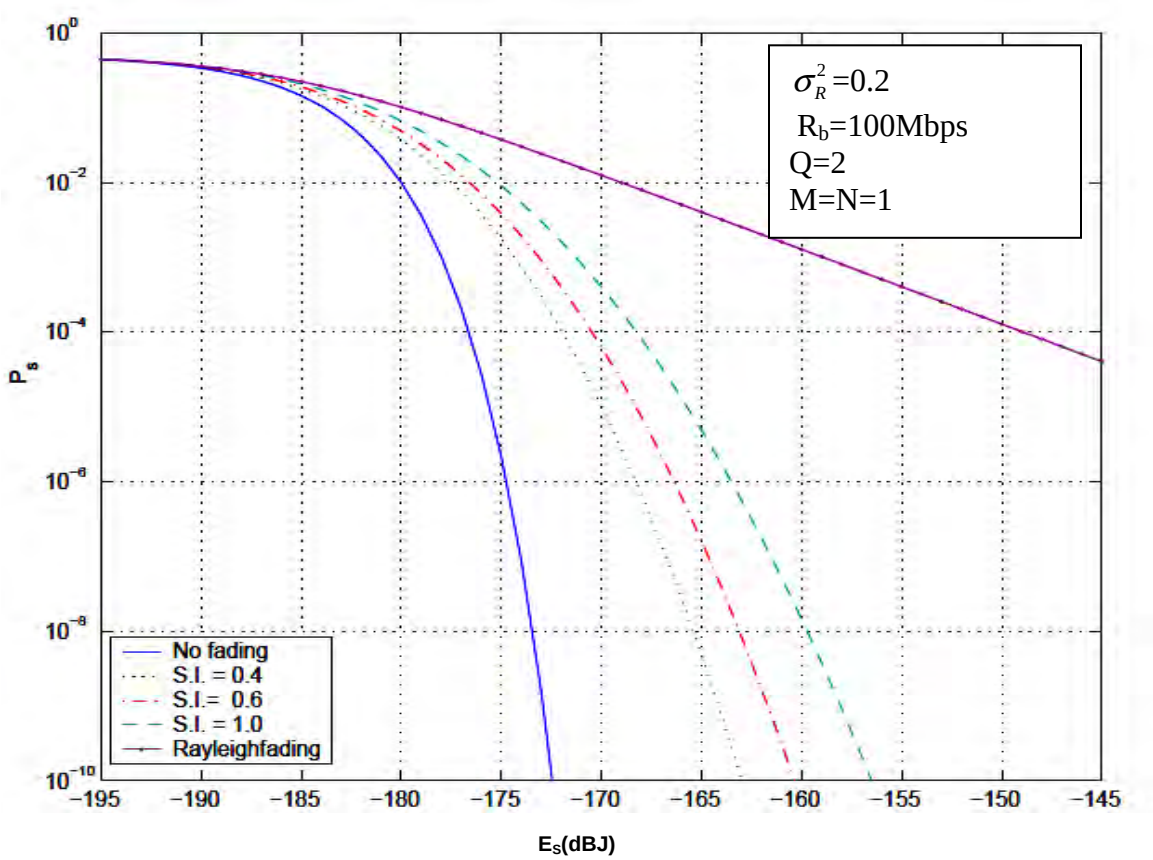

Fig-4.1: Symbol-error probability vs. symbol energy for Q=2, M=N=1 and no background noise, for lognormal channel with different S.I

Table 4.2: SEP for lognormal channel with different S.I

Condition	S.I	SEP at 10^{-10} (dBJ)
M=1 N=1 Q=2 and no background noise	0.4	-157
	0.6	-161
	1.0	-164
	No fading	-172.5

Following the analytical approach presented in section 3.4, the symbol error probability performance are evaluated at a data rate of 100Mbps. Keeping the others parameters are constant, we compare the performance of the system for Rayleigh fading and log-normal fading. Figure 4.1 shows the plot of symbol-error probability vs. symbol energy for Rayleigh fading and log-normal fading with varying the values of scintillation index by

using a single laser and photodetector. From Table 4.2 it is found that, the log-normal fading case causes degradation in system performance compared to the non-fading case.

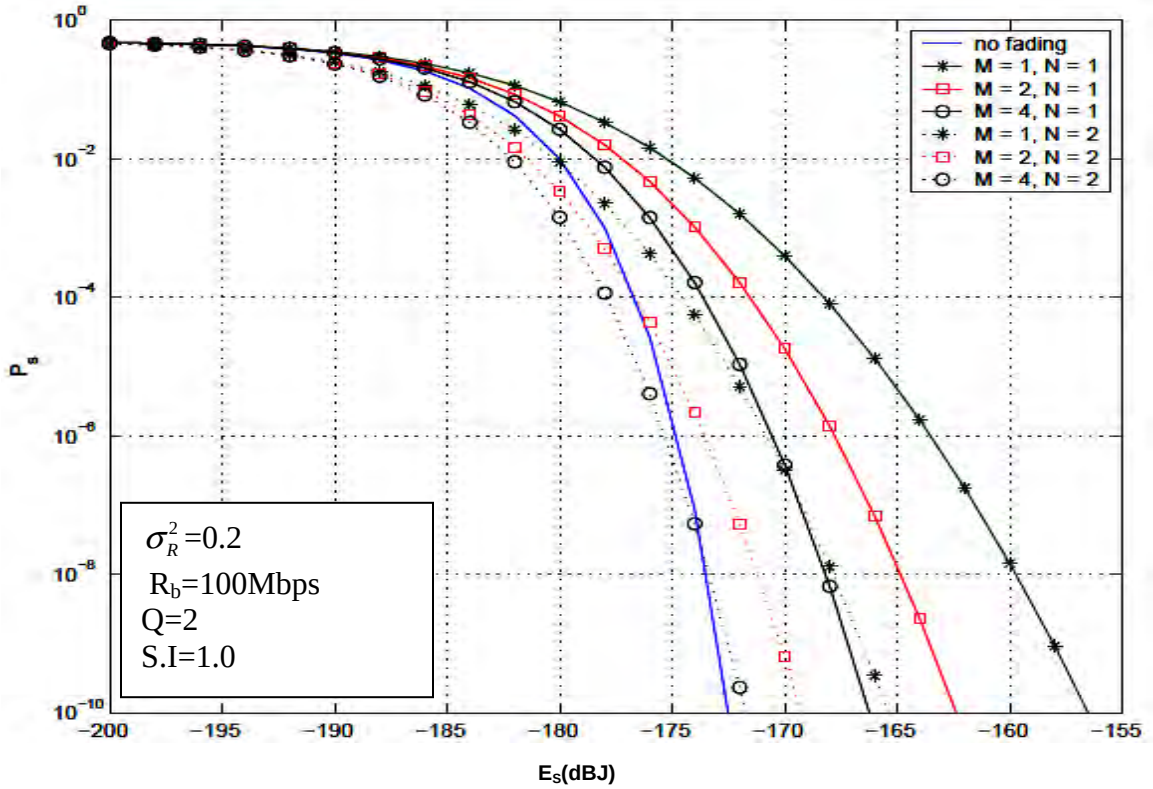

Fig-4.2: Symbol error probability vs. symbol energy for log-normal fading (S.I = 1.0), no background radiation, $Q = 2; M \in (1; 2; 4); N \in (1; 2)$

Table 4.3: SEP for lognormal channel with various combinations of transmitter and receiver.

No. of Transmitter	No. of Receiver	SEP at 10^{-10} (dBJ)
1	1	-157
2	1	-163
4	1	-166.5
1	2	-165
2	2	-169.25
4	2	-172

Fig. 4.2 shows the plot of symbol-error probability vs. symbol energy for log-normal fading with varying the no. of transmitting and receiving antennas. From Table 4.2 it is found that, the performance will improve if the no. of corresponding transmitter and receiver increases.

4.3.2 Numerical Result and Discussion for Gamma-gamma Channel

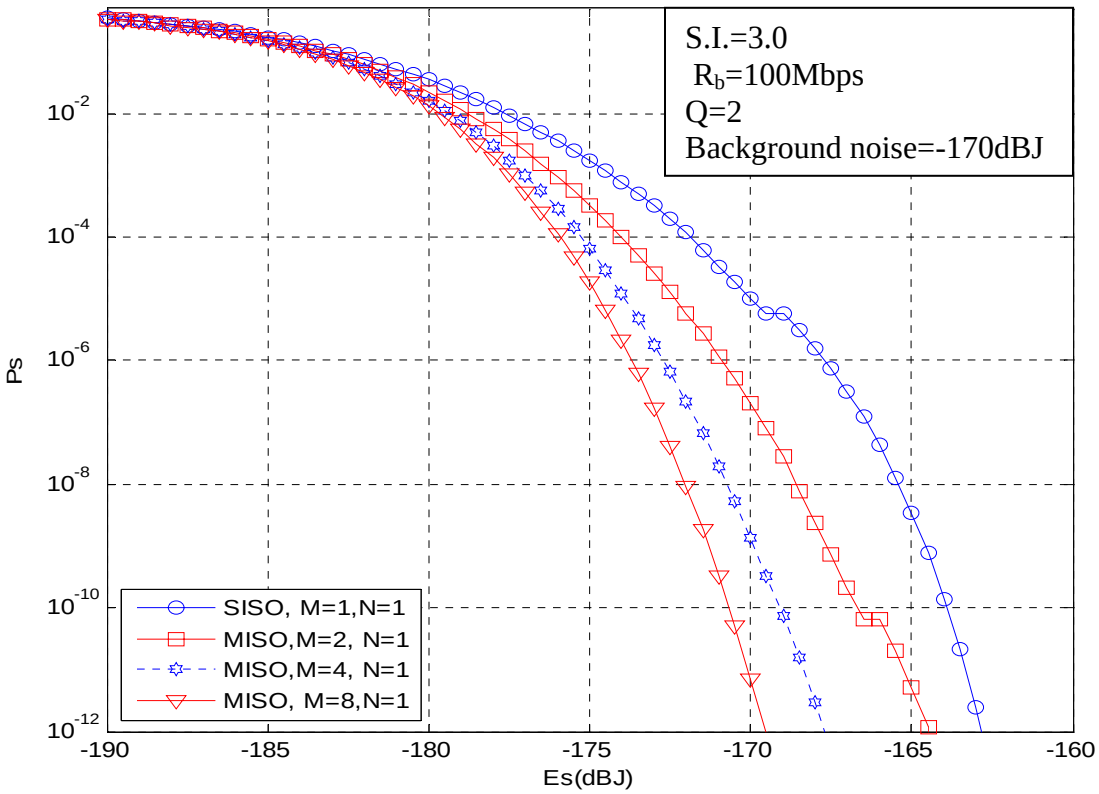

Fig-4.3: Symbol-error probability, for Q=2 with variable combination of M with S.I=3 for Gamma-gamma channel

Table 4.4: Symbol error probability for Gamma-gamma channel under various no. of transmitter.

No. of Transmitter	No. of Receiver	SEP at 10^{-12} (dBJ)
1	1	-163
2	1	-164.5
4	1	-168
8	1	-169.5

Fig. 4.3 shows the SEP P_s versus E_s where we have assumed quantum efficiency η=0.5. Table 4.4 shows the results for symbol error probability for gamma-gamma fading and fixed background radiation gamma-gamma by using a multiple laser and single photodetector. It is clearly found that, the SEP at 10^{-8} for single transmitter and receiver is -164 dBJ and it will improve more than 5dB for several combination of transmitter with single receiver.

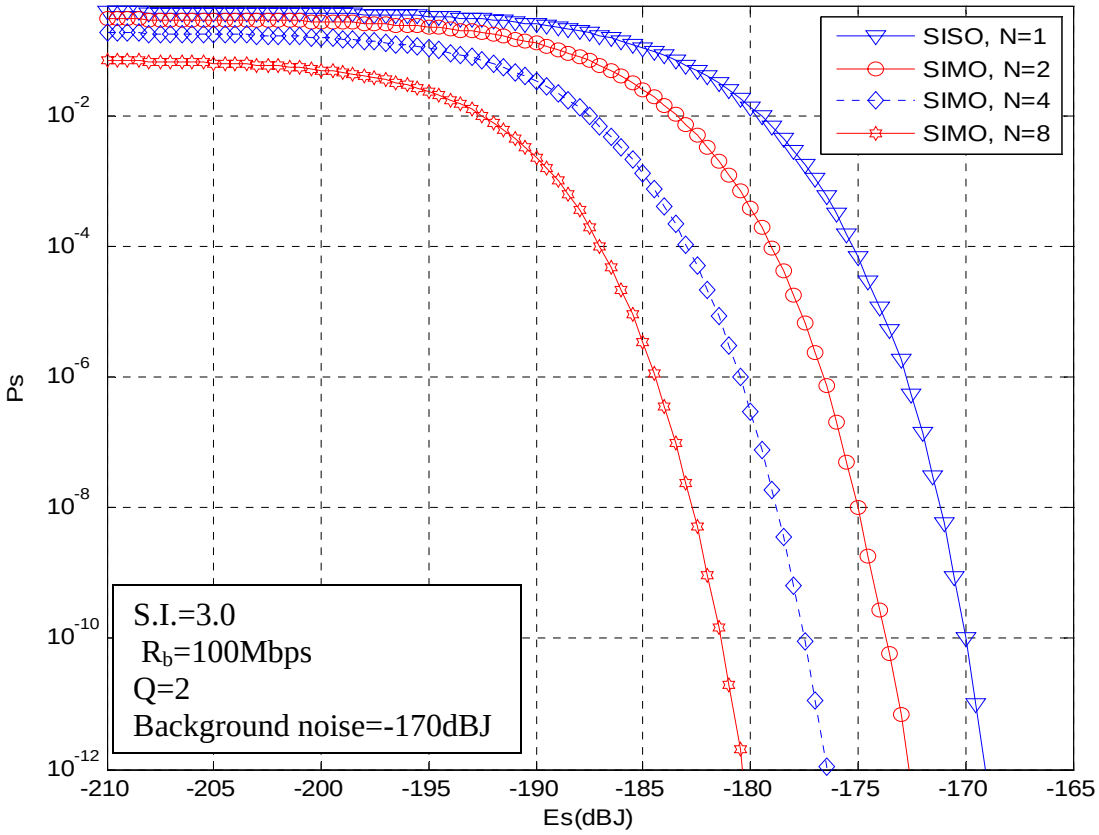

Fig-4.4: Symbol-error probability, for Q=2 with variable combination of N with S.I=3 for Gamma-gamma fading.

Fig 4.4 presents results for symbol error probability for gamma-gamma channel with constant value of scintillation index by using single laser and multiple photodetector. From the Table 4.5 it is clearly found that single lasers and multiple photodetector provides excellent performance in the case of symbol error probability compared to the single laser and multiple photodetector system.

Table4.5: Symbol error probability for Gamma-gamma fading under various no. of receiver.

No. of Transmitter	No. of Receiver	SEP at 10^{-12} (dBJ)
1	1	-169
1	2	-173
1	4	-177
1	8	-180.5

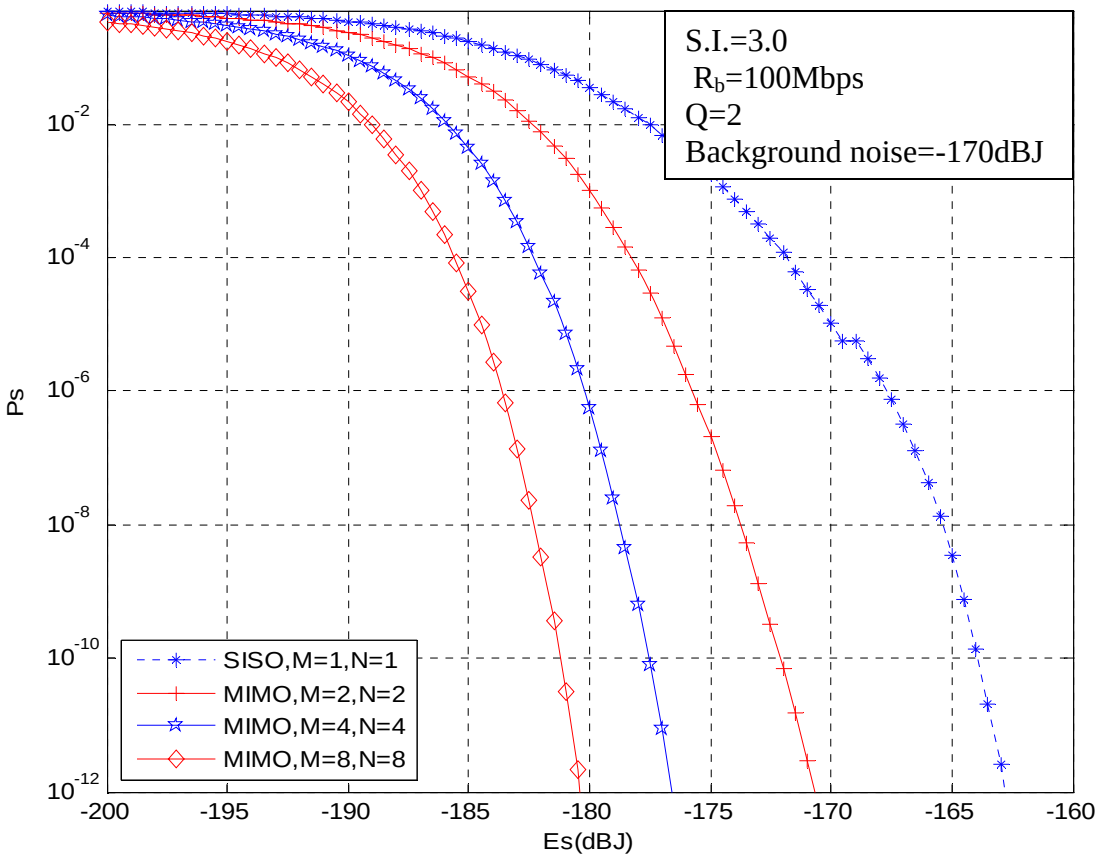

Fig-4.5: Plots of symbol-error probability vs. symbol energy for Q=2 with variable combination of M and N for Gamma-gamma fading (S.I = 3.0)

Fig. 4.5 shows the SEP versus E_s where we have assumed quantum efficiency η=0.5. The figure presents performance for binary PPM with gamma-gamma fading and fixed back ground radiation for an increasing the number of transmitter and receiver. Table 4.6 shows the advantage of using multiple transmitter and receiver in gamma-gamma channel.

Table 4.6: Symbol error probability under various no. of receiver for gamma-gamma fading.

No. of Transmitter	No. of Receiver	SEP at 10^{-12} (dBJ)
1	1	-163
2	2	-169
4	4	-177
8	8	-180.5

4.4 Performance Analysis of a LDPC Coded System with Q-ary PPM

4.4.1 Numerical Result and Discussion for Uncoded and LDPC Coded Modulation Scheme

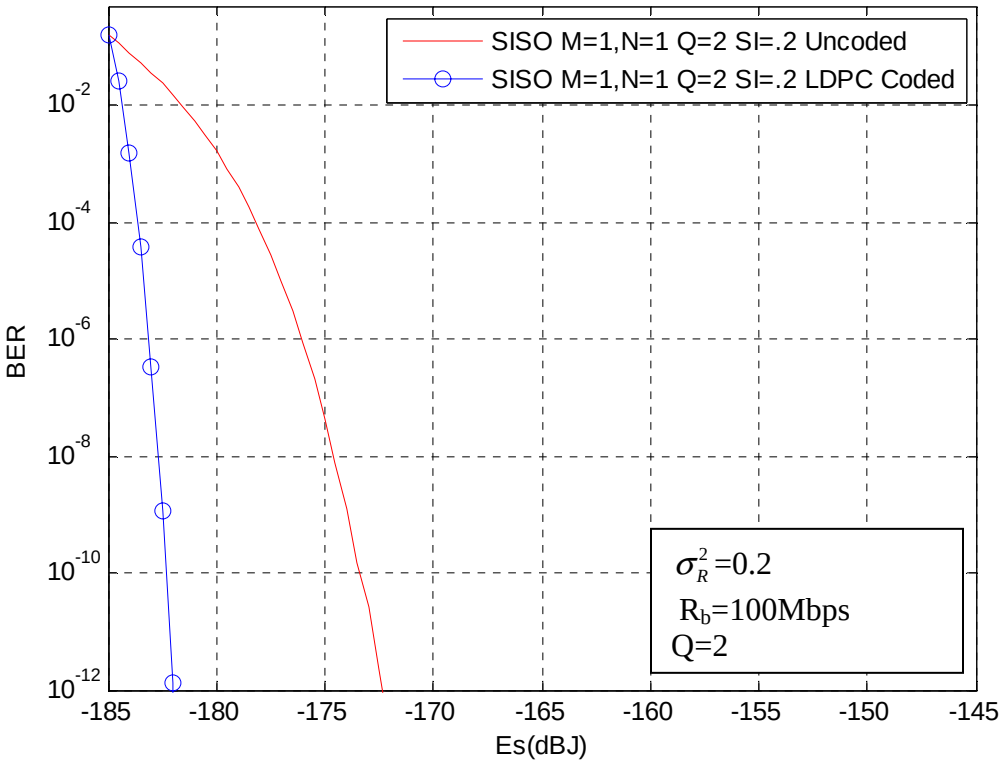

Fig-4.6: Plots of BER vs. symbol energy of uncoded and bit-interleaved LDPC-coded modulation scheme for FSO (SISO) communication with lognormal channel .

Fig 4.6 shows the plot of BER vs. symbol energy for lognormal fading with single transmitter and receiver under uncoded and energy efficient LDPC coded condition. The plot shows the improvement of BER for coded system than uncoded system. At a BER of 10^{-8} it is found that, it provides a coding gain of 8.5 dB under fixed background radiation. The amounts of improvement due to coding are shown in Table 4.7.

Table 4.7: BER Improvement due to coding for SISO system in lognormal channel.

No. of Transmitter	No. of Receiver	BER	Symbol energy(dBJ)	
			Uncoded	Coded
1	1	10^{-8}	-174.5	-183
		10^{-12}	-173	-182

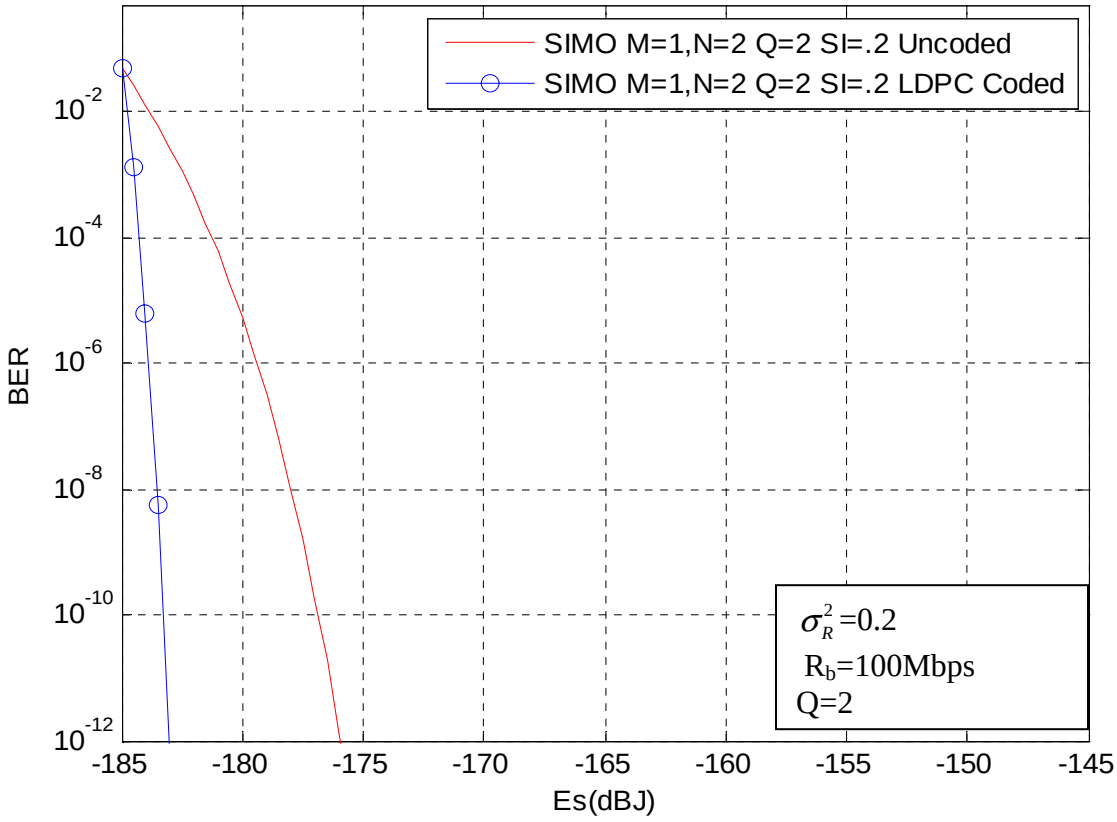

Fig-4.7: Plots of BER vs. symbol energy of uncoded and bit-interleaved LDPC-coded modulation scheme for FSO (SIMO) communication with lognormal channel .

Fig 4.7 shows the plot of BER vs. symbol energy for lognormal fading with single transmitter and multiple receiver under uncoded and LDPC coded condition. It can be seen that the BER in the order of 10^{-8} to 10^{-12} provides a coding gain of 6 to 7.5 dB respectively under fixed background radiation. The amounts of improvement due to coding are shown in Table 4.8.

Table 4.8: BER Improvement due to coding for SIMO system in lognormal channel.

No. of Transmitter	No. of Receiver	BER	Symbol energy(dBJ)	
			Uncoded	Coded
1	2	10^{-8}	-178	-184
		10^{-12}	-176	-183.5

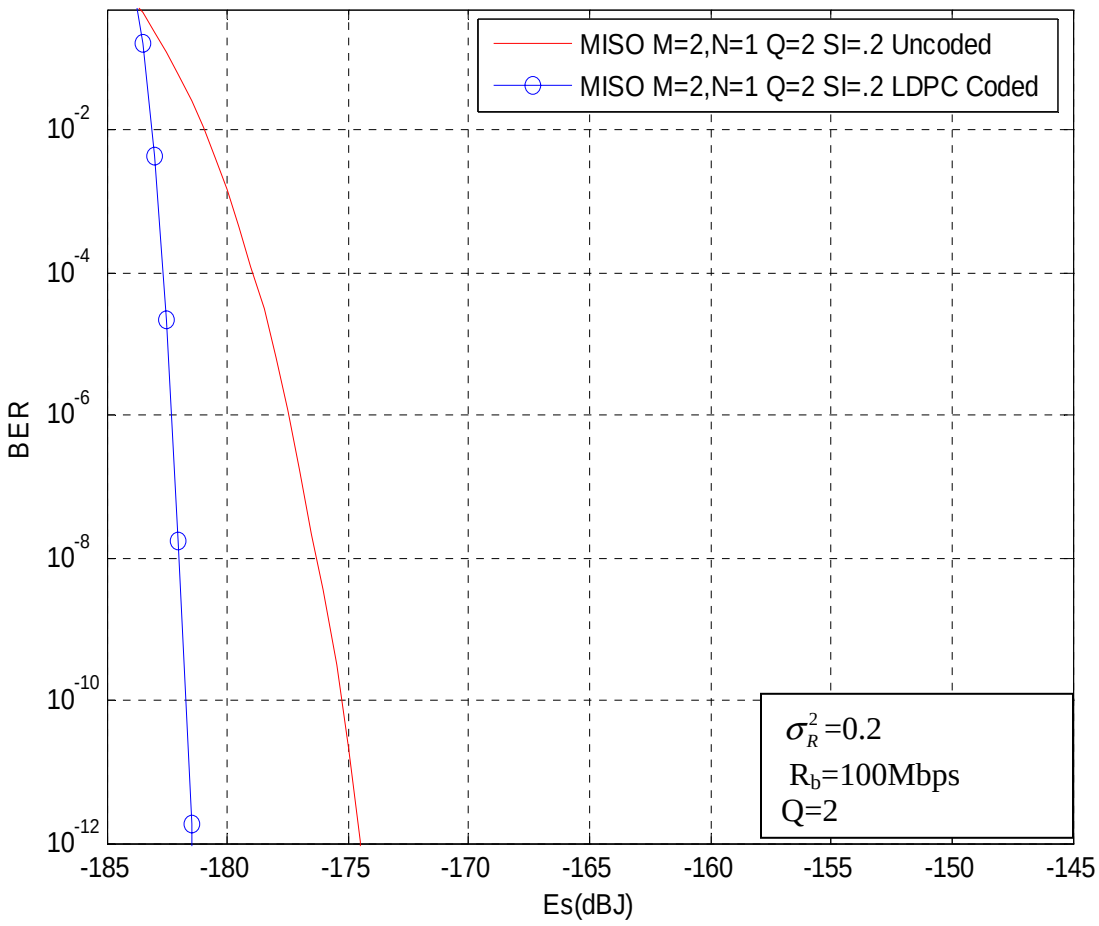

Fig-4.8: Plots of BER vs. symbol energy of uncoded and bit-interleaved LDPC-coded modulation scheme for FSO (MISO) communication with lognormal channel .

Fig 4.8 shows the plot of BER vs. symbol energy for lognormal fading with multiple transmitter and single receiver under uncoded and LDPC coded condition. It is noticed that BER performance is much better for coded system than uncoded system. The improvements in BER performance due to coding are shown in Table 4.9.

Table 4.9: BER Improvement due to coding for MISO system in lognormal channel.

No. of Transmitter	No. of Receiver	BER	Symbol energy(dBJ)	
			Uncoded	Coded
2	1	10^{-8}	-176.5	-182.5
		10^{-12}	-174	-182

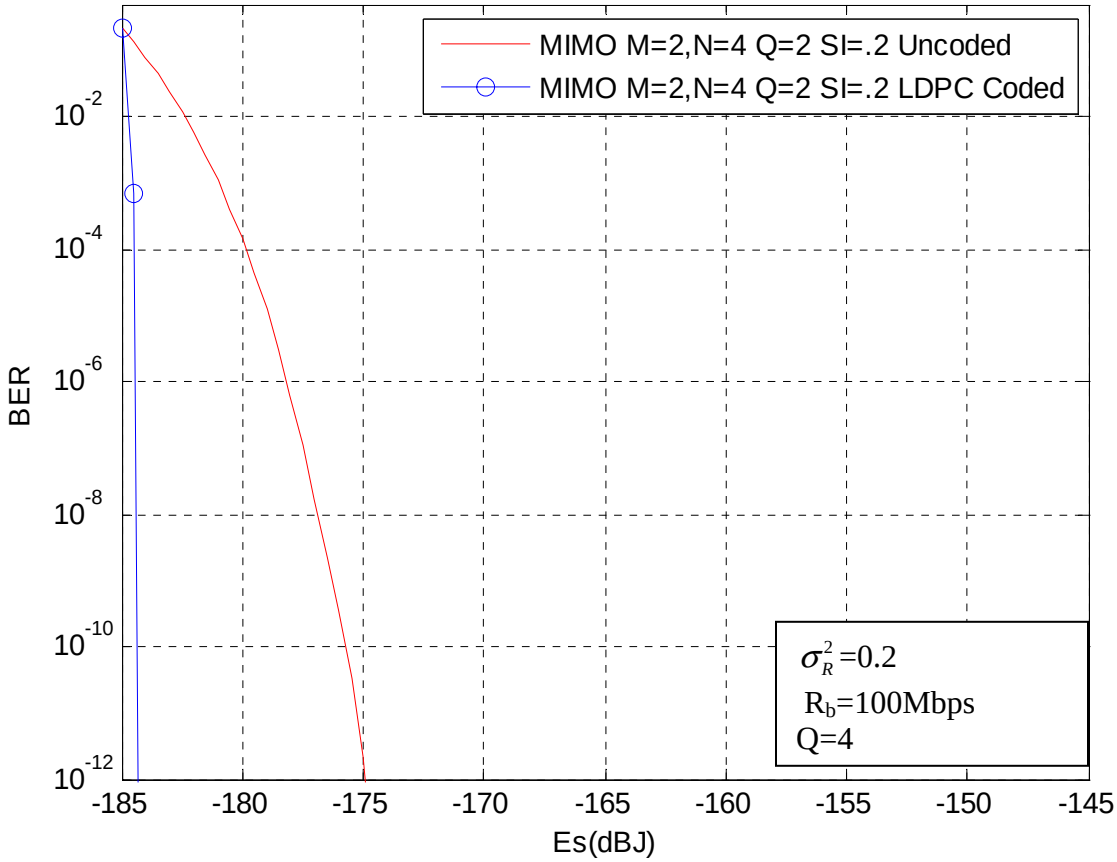

Fig-4.9: Plots of BER vs. symbol energy of uncoded and bit-interleaved LDPC-coded modulation scheme for FSO (MIMO) communication with lognormal channel .

Fig. 4.9 shows the Bit Error Rate (BER) vs. symbol energy for multiple no. of transmitter and receiver with constant background radiation under uncoded and coded condition. It is observed that the bit error performance is improved due to coding for MIMO system. For example, with constant background radiation a LDPC coded system provides significant coding gain of 8.5 to 10 dB over uncoded system at BER in the order of 10^{-8} and 10^{-12} respectively. The amounts of BER improvement due to coding are shown in Table 4.10.

Table 4.10: BER Improvement due to coding for MIMO system in lognormal channel.

No. of Transmitter	No. of Receiver	BER	Symbol energy(dBJ)	
			Uncoded	Coded
2	4	10^{-8}	-176	-184.5
		10^{-12}	-174.75	-184.5

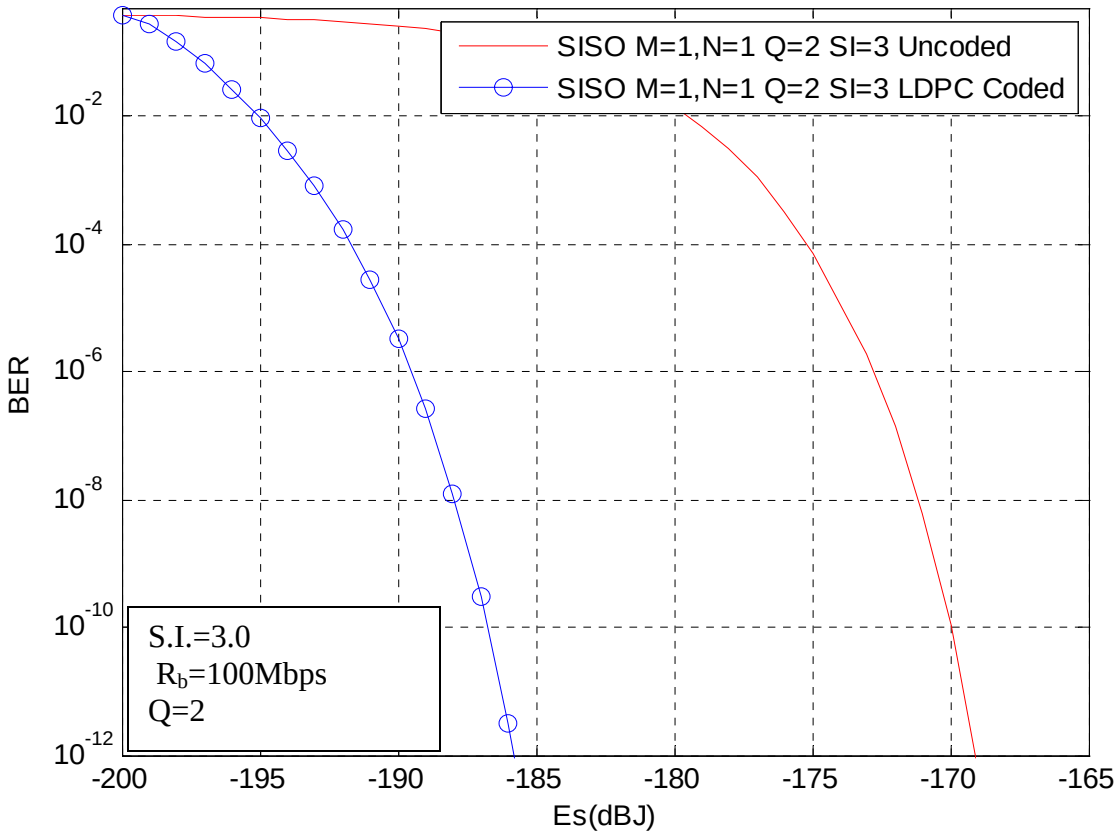

Fig-4.10: Plots of BER vs. symbol energy of uncoded and bit-interleaved LDPC-coded modulation scheme for FSO (SISO) communication with Gamma-gamma channel .

Fig. 4.10 shows the results for Bit Error Rate (BER) for gamma-gamma fading for single transmitter and receiver under uncoded and LDPC coded condition. From the figure it is seen that, it provides a coding gain of 17.5 dB at the BER in the order of 10^{-12} under fixed background radiation. The amounts of improvement due to coding are shown in Table 4.11.

Table 4.11: BER Improvement due to coding for SISO system in Gamma-gamma channel.

No. of Transmitter	No. of Receiver	BER	Symbol energy(dBJ)	
			Uncoded	Coded
1	1	10^{-8}	-172	-188
		10^{-12}	-168.75	-186.25

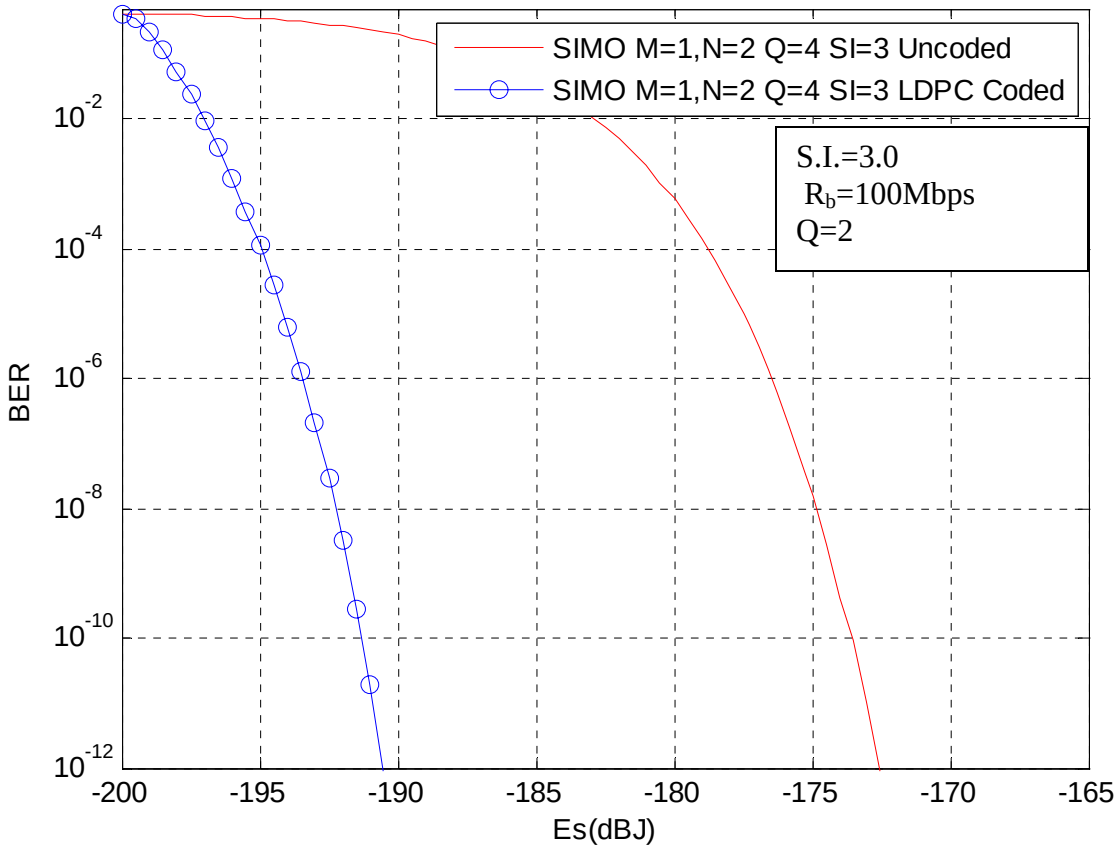

Fig-4.11: Plots of BER vs. symbol energy of uncoded and bit-interleaved LDPC-coded modulation scheme for FSO (SIMO) communication with Gamma-gamma channel .

Fig 4.11 shows the plot of BER vs. symbol energy for gamma-gamma fading with single transmitter and multiple receiver under uncoded and energy efficient coded condition. It shows that the BER in the order of 10^{-8} provides a coding gain of 17.5 dB under fixed background radiation. The amounts of improvement due to coding are shown in Table 4.12.

Table 4.12: BER Improvement due to coding for SIMO system with Gamma-gamma channel.

No. of Transmitter	No. of Receiver	BER	Symbol energy(dBJ)	
			Uncoded	Coded
2	1	10^{-8}	-175	192.5
		10^{-12}	-172.5	-191

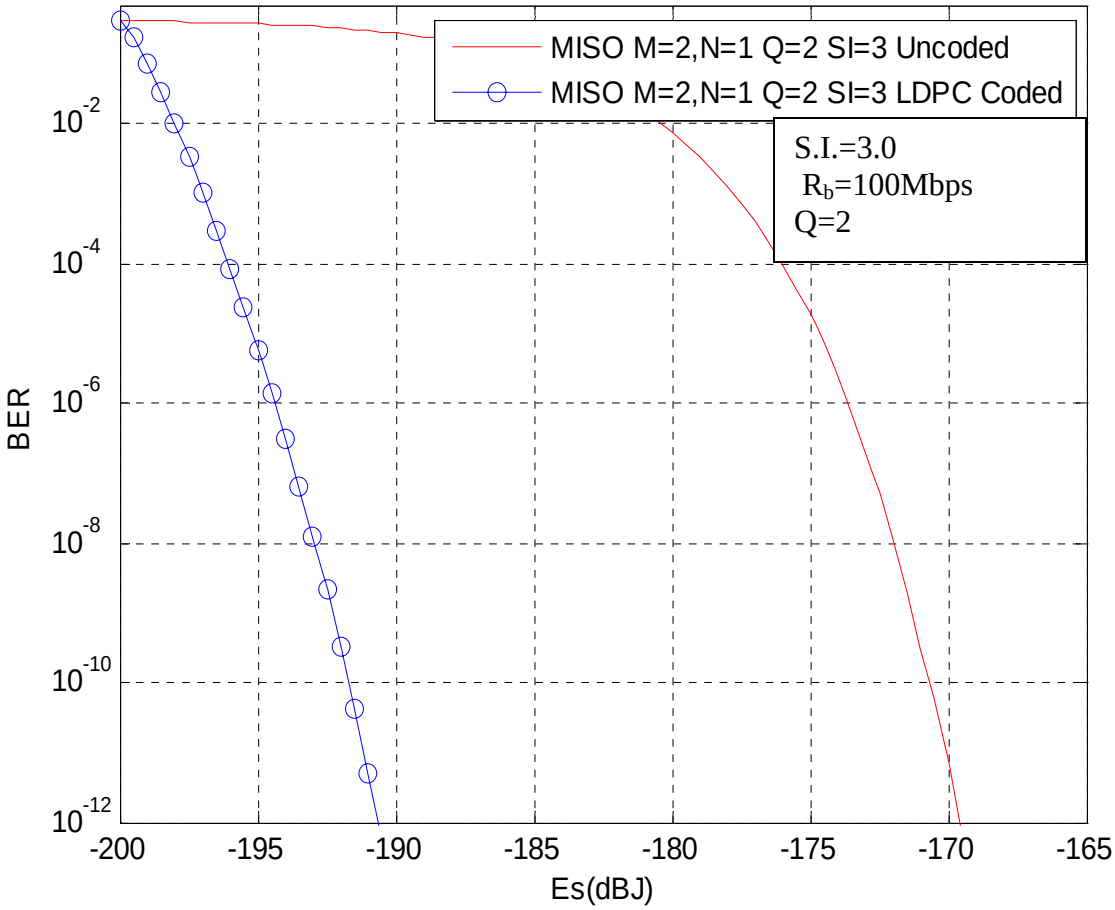

Fig-4.12: Plots of BER vs. symbol energy of uncoded and bit-interleaved LDPC-coded modulation scheme for FSO (MISO) communication with Gamma-gamma channel .

Fig 4.12 shows the results for symbol error probability for gamma-gamma fading and fixed background radiation for multiple transmitter and single receiver under uncoded and LDPC coded condition. Here we consider the no. of transmitter M=2 and the no. of receiver N=1, in such combination we found the coding gain of 21 dB at BER in the order of 10^{-12}. The BER performance due to coding are shown in Table 4.13

Table 4.13: BER Improvement due to coding for MISO system with gamma-gamma channel .

No. of Transmitter	No. of Receiver	BER	Symbol energy(dBJ)	
			Uncoded	Coded
2	1	10^{-8}	-172.5	-193
		10^{-12}	-169.75	-190.75

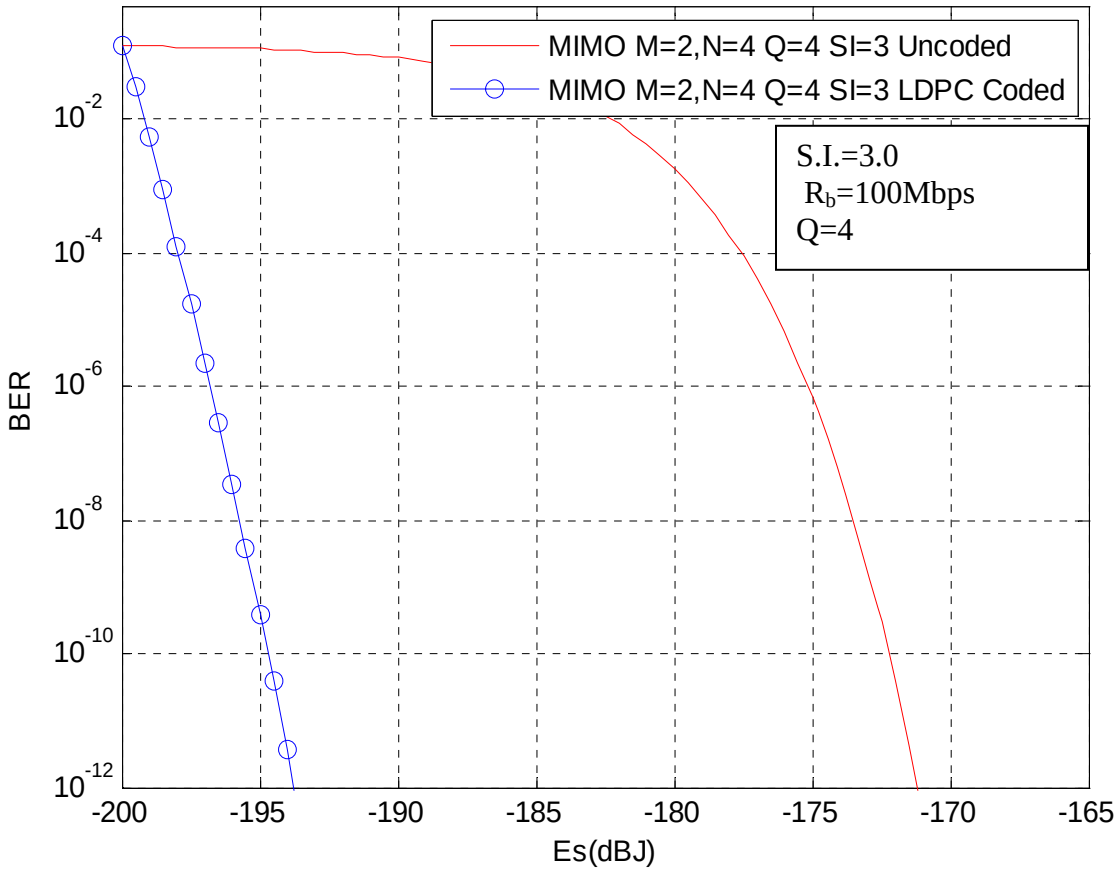

Fig-4.13: Plots of BER vs. symbol energy of uncoded and bit-interleaved LDPC-coded modulation scheme for FSO (MIMO) communication with Gamma-gamma channel .

Fig 4.13 shows the plot of BER vs. symbol energy for Gamma-gamma fading with multiple transmitters and multiple receiver under uncoded and LDPC coded condition. It shows that the BER in the order of 10^{-8} to 10^{-12} provides a coding gain of 21.5 to 22 dB respectively under fixed background radiation. The amounts of improvement due to coding are shown in Table 4.14.

Table 4.14: BER Improvement due to coding for MIMO system with gamma-gamma channel .

No. of Transmitter	No. of Receiver	BER	Symbol energy(dBJ)	
			Uncoded	Coded
2	4	10^{-8}	-174.5	-196
		10^{-12}	-172	-194

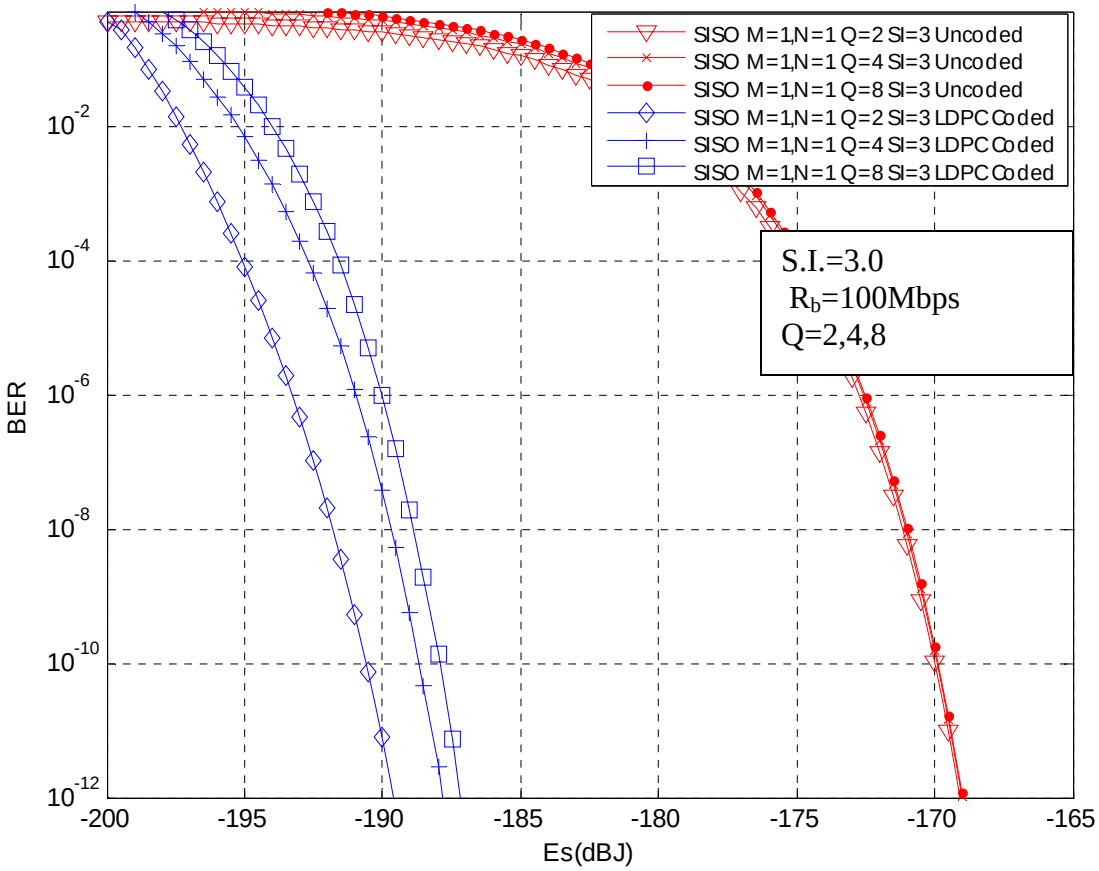

Fig-4.14: BER performance of bit-interleaved LDPC-coded modulation scheme for FSO (SISO) communication with strong turbulence strength.

Fig. 4.14 shows the BER performance under strong turbulence for SISO system with Q-ary scheme. The symbol energy due to background light is set to -170 dBJ. It is observed that the bit error performance is improved due to coding for SISO system. For example, with constant background radiation a LDPC coded system provides significant coding gain of 19 to 21 dB over uncoded system at BER in the order of 10^{-12} for different combination of Q. The amounts of improvement due to coding are shown in Table 4.15.

Table 4.15: BER Improvement due to coding with variable Q for SISO system.

No. of Transmitter	No. of Receiver	Q-ary	BER at 10^{-12}(dBJ)	
		(Q)	Uncoded	Coded
1	1	2	-168	-187
1	1	4	-168.25	-188
1	1	8	-168	-189.5

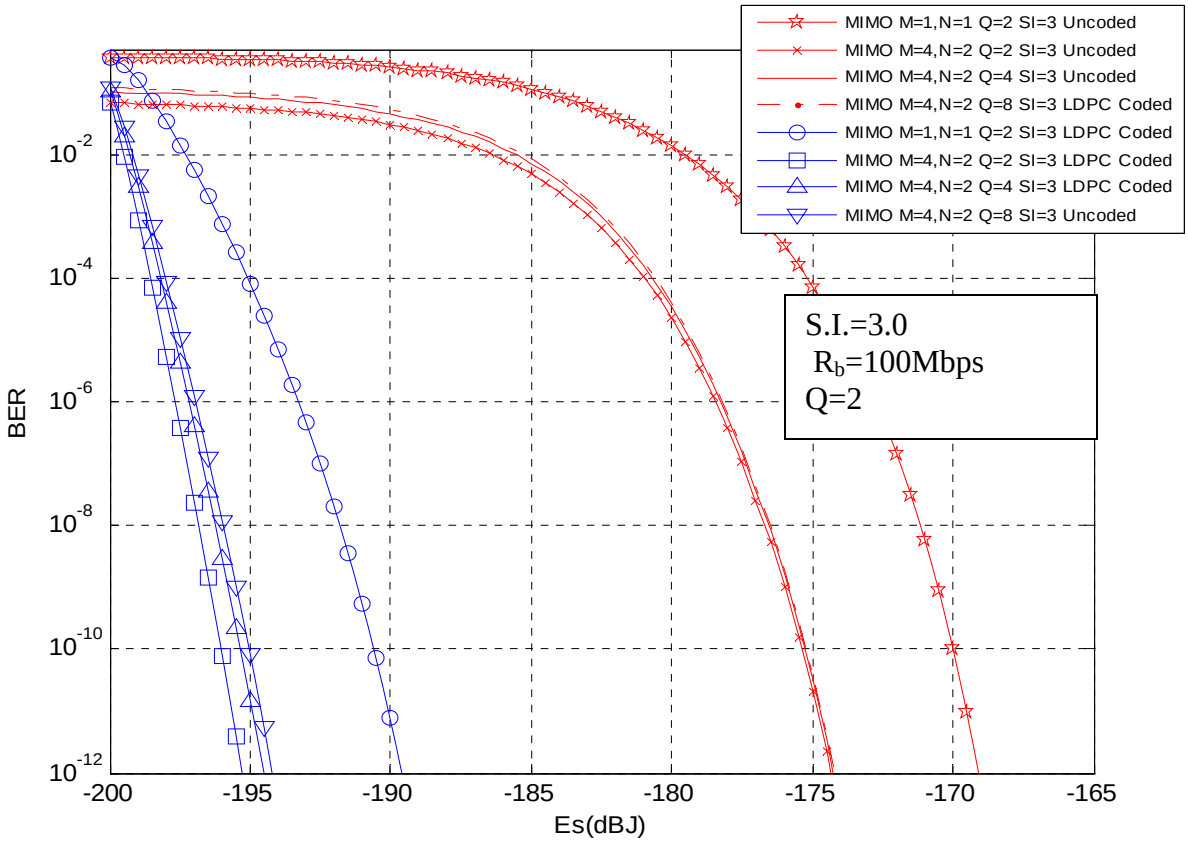

Fig-4.15: BER performance of bit-interleaved LDPC-coded modulation scheme for FSO (MIMO) communication with strong turbulence strength.

Fig. 4.15 shows the plot of BER vs. symbol energy performance for gamma-gamma fading with multiple transmitter and multiple receiver under uncoded and LDPC coded condition. with Q-ary scheme. The symbol energy due to background light is set to -170 dBJ for MIMO system. It is found that for MIMO configuration coded system provides better performance over uncoded system. It is also noticed that BER improves as the numbers of lasers and photodetectors are increased and in the presence of background light the BER decreases as the order of the Q-ary PPM scheme increases. The performance due to energy efficient coding are shown in Table 4.16

Table 4.16: BER Improvement due to coding with variable Q for MIMO system

No. of Transmitter	No. of Receiver	Q-ary (Q)	BER at 10^{-12}(dBJ)	
			Uncoded	Coded
1	1	2	-168	-187
4	2	2	-174	-193.5
4	2	4	-174	-196
4	2	8	174.5	194

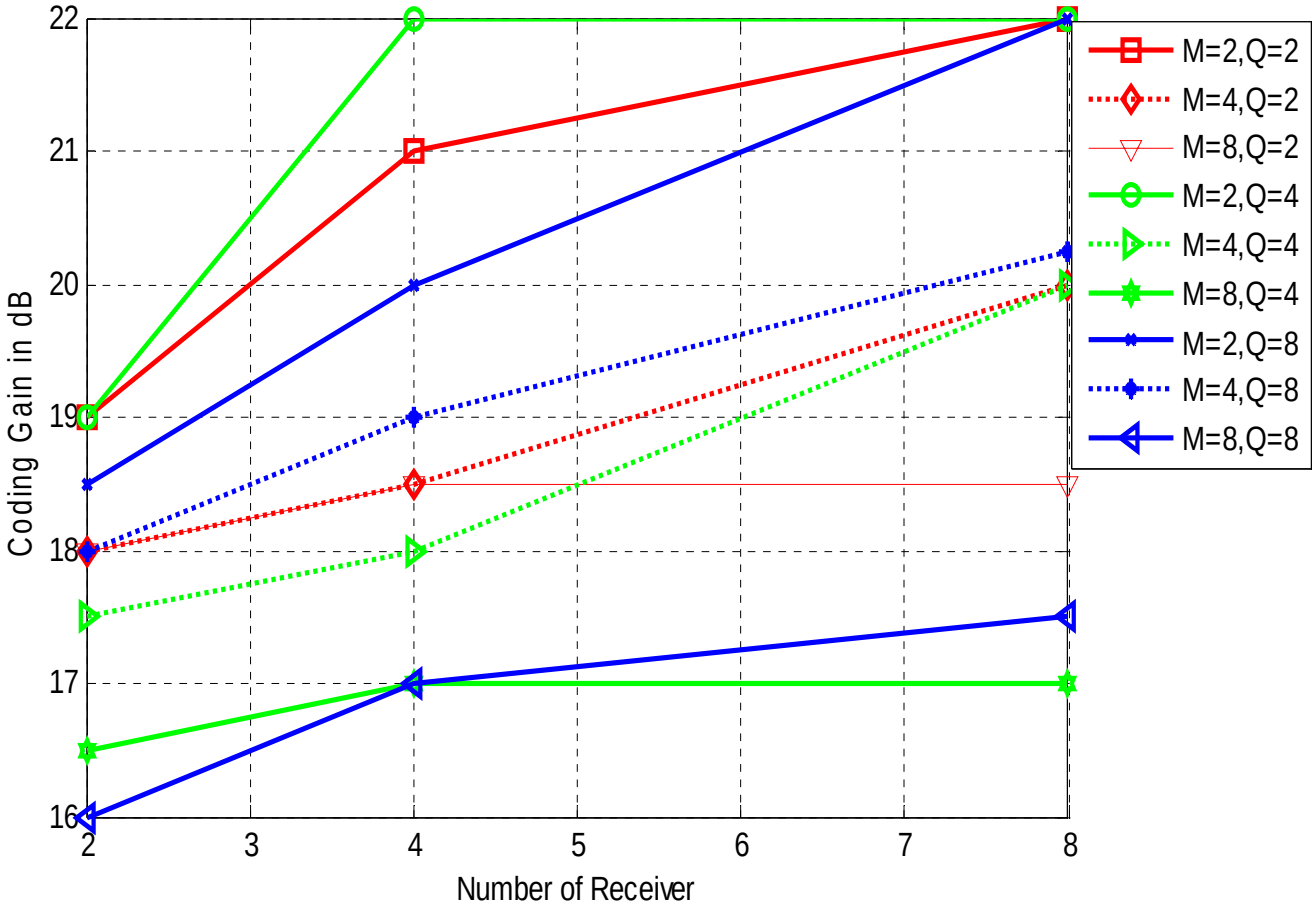

Fig-4.16: Plots of coding gain vs. number of receiver of LDPC-coded modulation scheme for FSO communication under strong turbulence strength with variable transmitter

Fig-4.16 shows the plot of coding gain vs. number of receiver of LDPC-coded modulation scheme The proposed LDPC coded scheme provides excellent coding gains for strong atmospheric turbulence conditions. For example, under strong turbulence the BICM scheme itself (for M=1,N=1,Q=2) provides a coding gain of 19 dB at BER of 10^{-12} The FSO MIMO system with M=2, N=4 Q=2 supplemented with BICM provides the 21 dB improvement at BER of 10^{-12} whereas the FSO MIMO system with M=2, N=4 Q=4 supplemented with BICM provides the 22 dB improvement at BER of 10^{-12} . Again the MIMO processing (M=2,N=4,Q=8) supplemented with BICM provides the 20 dB improvement at BER of $10^{-12.}$ The amounts of improvement due to coding are shown in Table 4.17.

Table 4.17: Coding gain determination with variable Q for MIMO system

No. of Transmitter (M)	No. of Receiver (N)	Q-ary (Q)	Coding Gain(dB)
2	2	2	19
2	4	2	21
2	8	2	22
4	2	2	18
4	4	2	18.5
4	8	2	20
8	2	2	18
8	4	2	18.5
8	8	2	18.5
2	2	4	19
2	4	4	22
2	8	4	22
4	2	4	17.5
4	4	4	18
4	8	4	20
8	2	4	16.5
8	4	4	17
8	8	4	17
2	2	8	18.5
2	4	8	20
2	8	8	22
4	2	8	18
4	4	8	19
4	8	8	20.25
8	2	8	16
8	4	8	17
8	8	8	17.5

4.5 Summary

Analytical results are presented considering the effect of atmospheric turbulence. We have considered the use of the lognormal distribution for weak turbulence and Gamma-gamma distribution for strong turbulence. From the over all analysis it is noticed that the BER performance is much better for coded system than uncoded system up to certain no. of transmitter and receiver. Various combinations of transmitter and receiver are performed to obtain maximum coding gain but the optimum coding gain is found with M=2, N=4 Q=4. The simulations are performed for up to 25 iterations in LDPC decoder. It is also found that the validity of lognormal distribution is limited to very weak turbulence but the gamma–gamma distribution fits even better than the log-normal distribution in the weak turbulence regime.

Chapter 5

Conclusion and Future work

Conclusion and Future work

5.1 Conclusion

Free space optics communication has emerged as a technology that has the potential to bridge the last-mile gap that separates homes and businesses from high speed access to the Internet. Atmospheric turbulence causes significant transmission impairment for an open air optical communication system and free space optical communication through atmosphere turbulence is analyzed under this research. A detailed analytical approach is presented to evaluate the bit error rate performance degradation of wireless optical link in the presence of atmospheric scintillation with Q-ary PPM schemes. The analysis is performed for different turbulence channel like log-normal and gamma-gamma channel and extended to evaluate the bit error rate performance of a free space optical link using LDPC coded over atmospheric turbulence channel. Performance results are evaluated for several combinations of transmitter and receiver. The essential contributions of the thesis are discussed below.

The gamma-gamma model approaches for heavy turbulence the exponential distribution, whereas in less turbulence it is suitable approximated by a lognormal distribution. To describe weak turbulence lognormal channel analysis is appropriate but moderate or heavy turbulence condition gamma-gamma channel is more appropriate to characterize the turbulence condition.

It is found that the performance of FSO is very sensitive to atmospheric scintillation. There is a significant degradation in BER performance due to atmospheric scintillation and penalty is higher for higher value of scintillation variation.

It is also found that MIMO systems can significantly improve the BER performance and provide diversity gain over single-input single-output systems. Here we propose an analytical approach to evaluate the performance of uncoded and power efficient coded-modulation scheme based on bit interleaved coded modulation (BICM) with LDPC codes as component codes, suitable for the use in MIMO FSO systems with Q-ary PPM. The bit-error rate (BER) performance results are evaluated with and without LDPC code in the presence of background radiation.

The performance results are evaluated numerically in terms of bit error rate (BER). It is observed that, the bit error performance is improved due to coding for MIMO system. For example, with constant background radiation a LDPC coded system provides significant coding gain of 21.5 to 22 dB over uncoded system at BER in the order of 10^{-8} and 10^{-12} respectively. Again various combinations of transmitter and receiver are performed to obtain maximum coding gain but the optimum coding gain is found with M=2, N=4 Q=4. The improvements due to LDPC code over the uncoded systems are evaluated and optimum system design parameters are also determined. Furthermore, the presented analytical approach also provides a number of advantages. For example it provides excellent coding gain, it also provides high power efficiency.

Finally power efficient coded-modulation scheme based on bit interleaved coded modulation (BICM) with LDPC codes provide excellent performance and easier to implement, because it requires the use of only one LDPC encoder/decoder.

5.2 Scope of Future Research work

Many extensions to this work can be made.

- A more accurate analysis of the proposed system would include thermal noise which has been ignored in this thesis.

- An important restriction on the implementation of LDPC codes is the block length which is restricted by the sector size of the storage device being used. Typical block lengths of this thesis do not exceed 5000 bits. A good extension for this work will be finite length analysis of this improved decoding algorithm. Pseudo-codeword analysis will be a good starting point.

- Research can be initiated to investigate the performance bounds of FSO link for different type of receiver in atmospheric turbulence

References

[1] X. Zhu and J. Kahn, "Communication techniques to mitigate atmospheric *and E turbulence* in free-space optical links," *The 16th Annual Meeting of the IEEE Lasers electro-Optics Society, 2003. LEOS 2003*, vol. 1, pp. 89–90, October 2003.

[2] Cvijetic N., Wilson S.G., and Brandt- Pearce M., "Receiver optimization in turbulent free-space optical MIMO Channels with APDs and Q-ary PPM,"*IEEE photon tehnol.Lett.18*, pp. *1491-1493 (2006)*

[3] Wilson S.G., Brands-Pearce M., Cao Q., and Leveque J.J.H.,III, "Free-Space optical MIMO transmission with Q-ary PPM," *IEEE Trans. Commun.53*, pp.*1402-1412 (2005)*

[4] Djordjevic I.B., Sankaranarayanan S., Chilappagari S. K, and Vasic B., "Low- density parity- check codes for 40 Gb/s optical transmission systems," *IEEE J. Sel. Top. Quantum Electron. 12*, pp. *555-562 (2006)*

[5] Djordjevic I.B., Vasic B., and Niefeld M. A., " Multilevel coding in free-space optical MIMO transmission with Q-ary PPM over the atmospheric turbulence channel," *IEEE Photon Technology.Lett.18*, pp. *1491-1493 (2006)*

[6] Djordjevic I.B., Vasic B., and Niefeld M. A., " Power efficient LDPC coded modulation for free-space optical communication over the atmospheric turbulence channel," *in Proc. OFC 2007, Paper on JthA46,March25-29, 2007, Anaheim, CA,USA.*

[7] Jilei Hou, Paul H. Siegel, LaurenceB. Milstein, and Henry D. Pfister, "Multilelevel Coding with Low- Density Parity-Check Components Codes", *IEEE (2001)*

[8] Djordjevic I.B., LDPC-coded MIMO optical communication over the atmospheric turbulence channel using Q-ary pulse position modulation. Opt. Express 16, pp.10026-10032(2007)

[9] X. Zhu and J. Kahn, "Free-space optical communication through atmospheric turbulence channels," *IEEE Trans. on Communications*, no. 2, pp. 1293–1300, 2003.

[10] S. B. Alexander, *Optical Communication Receiver Design*, vol. T22. SPIE Optical Engineering Press, 1997.

[11] Djordjevic I.B., Vasic B., and Niefeld M.A., "LDPC coded OFDM over the atmospheric turbulence channel," *Opt Express 15,* pp. *6332-6346 (2007)*

[12] H. Willebrand and B. Ghuman, "Fiber optics without the fiber," *IEEE Spectrum*, August 2001.

[13] G. Keiser, *Optical Fiber Communications*. McGraw-Hill, third ed., 2000.

[14] S. Hranilovic, Wireless Optical Communication Sysstem, Springer,2005. J. E. Padget, C. G. Gunther and T. Hatori , "Overview of wireless personal communications, "IEEE Commun.Mag.,vol.33,no. 1,pp.28-41, 1995

[15] J.M. Khan and J.R. Barry. "Wireless infrared communications." Proceedings of the IEEE, 85(2):2263-298, February 1997

[16] J.B. Carruthers and J.M. Khan. "Modeling of nondirected wireless infrared channels". IEEE Transactions on Communications, vol.45, no.10,pp.1260-1268, october1997.

[17] M. R. Pakravan, M. Kavehrad, and H. Hashemi. “Indoor wireless infrared channel characterization by measurements”. IEEE transactions on vehicular Technology, vol.50,no.4,pp.1053-1073, July 2001

[18] G. Yun and M. Kavehrad, “Spot-diffusing and fly-eye receivers for indoor infrared wireless communications”, In Proceedings of the IEEE international conference on selected topics in Wireless Communications,pp.262-265, 1992

[19] J. B. Carruthers and J. M. Khan,“ Angle diversity for nondirected wireless infrared communication”, IEEE Transactions on Communications, vol.48, no. 6, pp.960-969, June 2000.

[20] V. Jungnickel, A. Forck, T. Haustein, U. Krger, V. Pohl, and C. Von Helmolt, “Electronic tracking for wireless infrared communications.” IEEE Transactions on Wireless Communications , vol.2, no. 5, pp. 989-999, September 2003.

[21] E. Shin and V. Chan, “Optical communication over the turbulent atmospheric channel using spatial diversity,” *IEEE Conference on Communication*, pp. 2055–2060, 2002.

[22] I. S. C. Davis and S. Milner, “Flexible optical wireless links and networks,” *IEEE Communications Magazine*, vol. 41, pp. 51–57, March 2003.

[23] A. Acampora, “Last mile by laser,” *Scientific American*, June 17 2003.

[24] M.A. Al-Habash, L.C. Andrews, and R. L. Phillips, Optical Engineering 40,pp.1554- 1562 (2001).

Appendix-A

Bit Error Rate (BER) for Q-ary PPM:

The probability of error or bit error rate (BER) is given by-

$$P_s = \int P_{s|A} f(I) dI = \frac{Q-1}{Q} \left\{ \left[\int e^{-\frac{a^2 \eta \left(\frac{E_S}{M}\right)}{hf}} f(I) dI \right]^N \right\}^M \quad \text{(A.1)}$$

$$f(I) = \frac{2(\alpha\beta)^{(\alpha+\beta)/2}}{\Gamma(\alpha)\Gamma(\beta)} I^{\frac{(\alpha+\beta)}{2}-1} K_{(\alpha-\beta)}(2\sqrt{\alpha\beta I}), I > 0 \quad \text{(A.2)}$$

where,

I =the signal intensity

$\Gamma(.)$ = the gamma function, and

$K_{(\alpha-\beta)}$ = modified Bessel function of the second kind and order $(\alpha-\beta)$.α and β are PDF parameters describing the scintillation experienced by plane waves, and in the case of zero-inner scale.

α and β are given by,

$$\alpha = \frac{1}{\exp\left[\frac{0.49\sigma_R^2}{(1+1.11\sigma_R^{12/5})^{7/6}}\right]-1} \quad \text{(A.3)}$$

$$\beta = \frac{1}{\exp\left[\frac{0.51\sigma_R^2}{(1+0.69\sigma_R^{12/5})^{5/6}}\right]-1} \quad \text{(A.4)}$$

$$\boldsymbol{\sigma_R^2 = 1.23 C_n^2 k^{7/6} L^{11/6}} \quad \text{(A.5)}$$

where C_n^2 is the wave number spectrum structure parameter, which is altitude-dependent.

Appendix-B

Matrix Representation for LDPC codes

For a matrix to be called low-density the two conditions wc << n and wr << m must be satisfied. In order to do this, the parity check matrix should usually be very large, so the example matrix can't be really called low-density.

$$H = \begin{bmatrix} 0 & 1 & 0 & 1 & 1 & 0 & 0 & 1 \\ 1 & 1 & 1 & 0 & 0 & 1 & 0 & 0 \\ 0 & 0 & 1 & 0 & 0 & 1 & 1 & 1 \\ 1 & 0 & 0 & 1 & 1 & 0 & 1 & 0 \end{bmatrix} \quad \text{(B.1)}$$

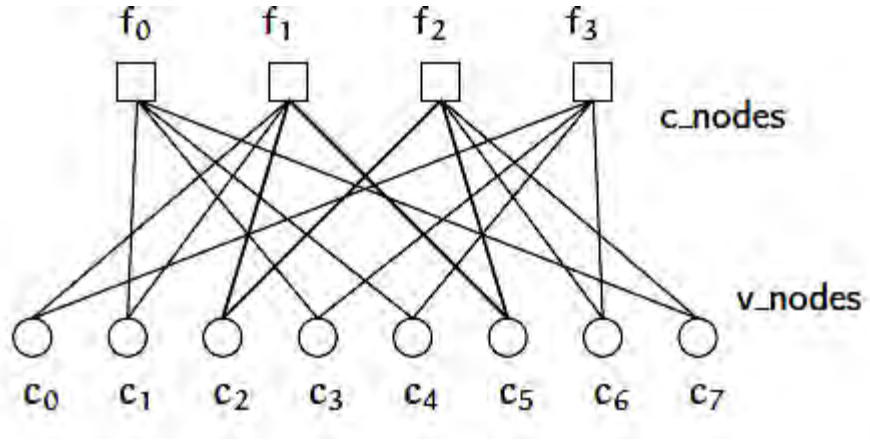

Figure 1: Tanner graph corresponding to the parity check matrix in equation (B.1). The marked path $c_2 \rightarrow f_1 \rightarrow c_5 \rightarrow f_2 \rightarrow c_2$ is an example for a short cycle. Those should usually be avoided since they are bad for decoding performance

Appendix-C

BER Analysis for LDPC Coded system

The outputs of the N receivers in response to symbol q, denoted as Zn,q (n=1,2,…,N; q=1,2,…,Q), are processed to determine the symbol reliabilities $\boldsymbol{\lambda(q)}$ (q=1,2,…,Q) given by

$$\lambda(q) = -\frac{\sum_{n=1}^{N}\left(Z_{nq} - \frac{\sqrt{E_s}}{M}\sum_{m=1}^{M} I_{n,m}\right)^2}{\sigma^2} - \frac{\sum_{n=1}^{N}\sum_{1\neq q}^{Q} Z_{n,I}}{\sigma^2} \qquad \text{(C.1)}$$

where,

$\boldsymbol{E_s}$= symbol energy of uncoded symbol in electrical domain (in the absence of scintillation).

$\boldsymbol{\sigma^2 = N_0/2}$ = the variance of TA thermal noise (that is modeled as additive white Gaussian noise (AWGN).

$\boldsymbol{I_{nm}}$ = intensity of the light incident to $\boldsymbol{n}^{\text{th}}$ photodetector (n=1,2,…,N), originated from $\boldsymbol{m}^{\text{th}}$ (m=1,2,…,M) laser source, which is described by the Gamma-Gamma probability density function (PDF).

The bit reliabilities $\boldsymbol{L(c_j)}$, (j=1,2,…,m) (cj is the jth bit in observed symbol q binary representation $\boldsymbol{c}$=(c_1,c_2,…,c_m)) are determined from symbol reliabilities are given by[2],

$$L\left(c_j\right) = \log\frac{\sum_{c:c_j=0}\exp\left[\lambda(q)\right]}{\sum_{c:c_j=1}\exp\left[\lambda(q)\right]}, \qquad \text{(C.2)}$$

Appendix-D

Table D.1 Channel Parameters For Capacity Computations for Q = 200.

σ_R	α	β	σ_I^2
0.2	45.79	41.55	0.0464
0.4	12.87	10.67	0.179
0.6	6.82	5.05	0.374
0.8	4.75	3.14	0.596
1.0	3.83	2.29	0.811
1.5	3.04	1.50	1.214
2.0	2.88	1.25	1.422
3.0	2.98	1.09	1.557
4.0	3.18	1.05	1.571
5.0	3.41	1.03	1.555
6.0	3.62	1.02	1.534
7.0	3.82	1.01	1.512
8.0	4.00	1.006	1.493
9.0	4.17	1.004	1.475
10.0	4.34	1.002	1.459

Coding Gain determination under different no. of transmitter and receiver

SIMO System

No. of Transmitter (M)	No. of Receiver (N)	Q-ary (Q)	Coding Gain(dB)
1	1	2	19
1	2	2	18.5
1	4	2	17
1	8	2	16
1	1	4	18.5
1	2	4	18
1	4	4	17.5
1	8	4	16
1	1	8	19
1	2	8	18
1	4	8	17
1	8	8	16

MISO System

No. of Transmitter (M)	No. of Receiver (N)	Q-ary (Q)	Coding Gain(dB)
1	1	2	17
2	1	2	21
4	1	2	22
8	1	2	23.5
1	1	4	18.5
2	1	4	19.5
4	1	4	20
8	1	4	23.5
1	1	8	19
2	1	8	19.5
4	1	8	20
8	1	8	22

MIMO System

No. of Transmitter (M)	No. of Receiver (N)	Q-ary (Q)	Coding Gain(dB)
2	2	2	19
2	4	2	21
2	8	2	22
4	2	2	18
4	4	2	18.5
4	8	2	20
8	2	2	18
8	4	2	18.5
8	8	2	18.5
2	2	4	19
2	4	4	22
2	8	4	22
4	2	4	17.5
4	4	4	18
4	8	4	20
8	2	4	16.5
8	4	4	17
8	8	4	17
2	2	8	18.5
2	4	8	20
2	8	8	22
4	2	8	18
4	4	8	19
4	8	8	20.25
8	2	8	16
8	4	8	17
8	8	8	17.5